ELSEVIER

Marine Geology 152 (1998) 295–324

MARINE GEOLOGY
INTERNATIONAL JOURNAL OF MARINE GEOLOGY, GEOCHEMISTRY AND GEOPHYSICS

The systematic contribution of transporting mechanisms to the cross-shore sediment transport in water depths of 3 to 9 m

B.G. Ruessink *, K.T. Houwman, P. Hoekstra

Department of Physical Geography, Institute for Marine and Atmospheric Research, University of Utrecht, P.O. Box 80115, 3508 TC Utrecht, Netherlands

Received 15 May 1998; accepted 17 July 1998

Abstract

The systematic contributions of short waves, infragravity waves and mean flows to the cross-shore sediment transport were studied with direct measurements of instantaneous near-bed sediment concentrations and velocities as well as with an energetics-based sediment transport model using measured time series of near-bed cross-shore flow as input. The study was conducted at four cross-shore positions in the multiple bar system of Terschelling, Netherlands during three field campaigns, each with a five-week duration. The data were collected in 3- to 9-m water depth during a wide range of conditions, from low-energy non-breaking conditions to almost fully saturated breakers. The height over depth ratio H_s/h was applied at all four measuring stations as a local conditional parameter. All model predictions were grouped into H_s/h classes with a width of 0.02 to highlight the generality of the data. The energetics approach predicted that the suspended load dominated over the bedload at all four stations. Both the sediment flux measurements as well as the model predictions showed that the largest contributors to the gross suspended sediment transport were made by the short waves and the undertow, inducing an onshore and offshore transport, respectively. Their contributions to the gross suspended transport were about 40 to 50% under surf zone conditions. Bound infragravity waves were observed and predicted to result in an offshore directed transport that was of subordinate magnitude compared to the observed and estimated magnitudes by the short waves and the undertow. However, as these transports almost cancelled out because of their about equal magnitude but opposite sign, the suspended transport by bound infragravity waves may not be ignored and may, rather paradoxically, have a relatively large influence on the net suspended sediment transport. Hydrodynamical processes that do not seem to be of importance to the onshore and offshore sediment transport in 3- to 9-m water depth in the long run are mean flows under non-breaking conditions and free infragravity motions. A direct comparison between measured sediment fluxes and the model predictions suggests that simple energetics models are suitable for predicting cross-shore sediment transport in 3- to 9-m water depth.

Keywords: nearshore environment; sediment transport; suspended sediments; bars

* Corresponding author. Tel.: +31 (30) 2533864; Fax: +31 (30) 2540604; E-mail: b.ruessink@geog.uu.nl

0025-3227/98/$19.00
PII: S0025-3227(98)00133-9

1. Introduction

Sand bars are common morphological features of sandy coasts. On the time scale of hours to weeks (hereafter referred to as small-scale) bars may move slowly onshore during low-energy conditions, whereas they typically migrate offshore rather rapidly during storm conditions (Sunamura and Takeda, 1984; Sallenger et al., 1985; Thornton et al., 1996; Gallagher et al., 1998). On a longer time scale (of about years; medium-scale) a cyclic behaviour has been observed (Ruessink and Kroon, 1994; Wijnberg and Terwindt, 1995; Shand and Bailay, 1998). A cycle consists of bar generation near the shoreline, net offshore migration and bar decay in the outer nearshore zone. The question whether it is possible to predict the medium-scale behaviour of bars and nearshore profiles in a quantitative way has still to be answered negatively, although promising model predictions have recently been presented by Roelvink et al. (1995). Most of our knowledge of small-scale processes that may drive medium-scale morphological change has been obtained by short, intense field campaigns, mathematical models and laboratory experiments, on time scales of hours to weeks. Hence there is a remarkable gap between the medium-scale morphological observations and the time scale of process knowledge. It has proved to be very hard to upscale the process knowledge to medium-scale profile evolution. If, in some way, the modelling of physical small-scale processes is applied in the prediction of medium-scale morphological development, it should obviously be known which small-scale processes are of importance in the long run. The present paper therefore focuses on the systematic contribution of various small-scale processes to the sediment transport based on a data set of several thousands of hours of field observations.

Small-scale hydrodynamical processes that have been identified as significant contributors to the cross-shore sediment transport in the nearshore zone include short waves (i.e., sea and swell), infragravity waves and mean cross-shore currents (e.g., Jaffe et al., 1984; Huntley and Hanes, 1987; Osborne et al., 1990; Osborne and Greenwood, 1992; Russell, 1993; Aagaard and Greenwood, 1994, 1995). Most field studies on sediment transport in the nearshore zone have shown that the onshore directed transport by short waves dominates the total particle flux under shoaling conditions (e.g., Beach and Sternberg, 1991; Osborne and Greenwood, 1992; Russell et al., 1995). Bound infragravity waves and mean flows seem to be of lesser importance. Under surf zone conditions, the largest contribution to the net cross-shore sediment transport is most often made by the wave-driven undertow; in addition, free infragravity motions may be of importance as well, especially on dissipative beaches (e.g., Beach and Sternberg, 1991; Russell, 1993; Aagaard and Greenwood, 1994, 1995; Russell et al., 1995). It has to be stressed that this general pattern, which has not yet been properly quantified, is based on observations made in water depths less than about 2 to 4 m. Whether it is also valid at larger depths, where we performed our measurements, is unknown.

The aim of this paper is to identify the systematic contributions of short waves, infragravity waves and mean flows to the cross-shore sediment transport. The term ‘systematic’ implies that we are more interested in the general pattern over a wide range of conditions than in the specific details of an individual measurement. In this paper the systematic contributions are analysed along two supplementary lines. In the first approach, the contributions are investigated with actual measurements of instantaneous near-bed concentration and velocity. Although the measured sediment fluxes provide valuable insight into the importance of various mechanisms to the onshore/offshore transport, there are obvious problems associated with this approach. For instance, the vertical resolution of the sediment fluxes is often poor, and as a consequence, the findings are not necessarily representative of the depth-integrated cross-shore sediment fluxes. In addition, there is the problem of the importance of bedload versus suspended load. Obviously, measurements of instantaneous near-bed velocity and concentration only consider the suspended load; bedload cannot be measured successfully in the field at present. Accordingly, we turn to simple energetics-based sediment transport modelling in the second approach to handle (at least partly) the afore-mentioned problems associated with the sediment flux approach.

2. Field site, instrumentation and observations

The data analysed in this paper were collected from the multiple bar system at Terschelling, Netherlands, during three campaigns, each with a five-week duration. Terschelling is a 30-km-long, approximately east–west-oriented barrier island in the northern part of the Netherlands and is fully exposed to the semi-enclosed North Sea. The three campaigns were conducted in May–June 1994, October–November 1994 and October–November 1995, and are hereafter referred to as the T2-, T3- and T4-campaign, respectively.

Fig. 1 shows the cross-shore profile of the measurement section at the onset of each campaign, together with the instrumented positions. The distance of the instrumented positions with respect to the shoreline as well as their mean water depth is presented in Table 1. As can be seen, the nearshore zone is characterised by a multiple bar system. During the T4-campaign the middle bar zone (say, between 400 and 800 m from the shoreline) in the vicinity of the measurement section was highly irregular in the alongshore direction; the middle bar consisted of several 'drumstick'-shaped parts with a longshore width of the order of 1 km. Position P3 was located in a channel between two of these 'drumstick'-shaped bars (Ruessink, 1998a). During the two previous campaigns the middle bar was more uniform in the alongshore direction; a channel

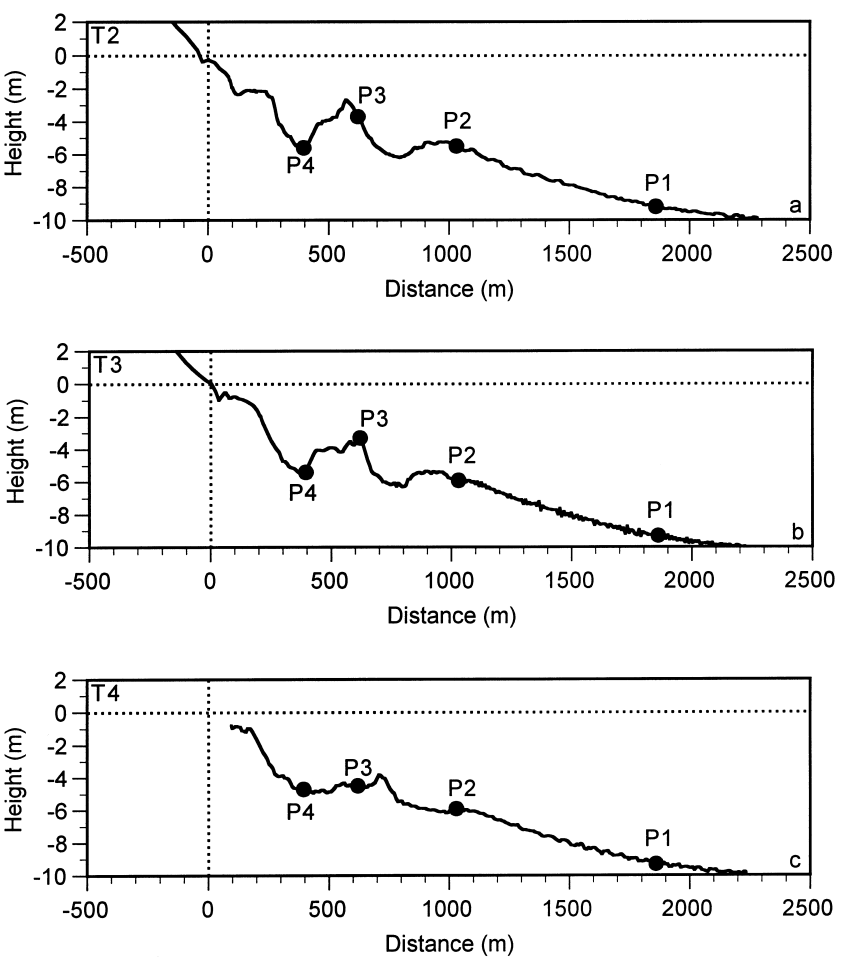

Fig. 1. Cross-shore profile of the measurement section at the onset of the (a) T2-campaign, (b) T3-campaign and (c) T4-campaign. Height is with respect to NAP (= Dutch Ordnance Level; 0 m NAP is about mean sea level).

Table 1
Location of instrumented tripods

	Distance to shoreline[a] (m)	Height (m NAP)		
		T2	T3	T4
P1	1860	−9.2	−9.2	−9.2
P2	1030	−5.5	−5.9	−5.9
P3	640	−3.7	−3.3	−4.5
P4	395	−5.6	−5.4	−4.7

[a] Shoreline is isoline of 0 m NAP (about mean sea level).

through the straight middle bar crest was observed close to the measurement array during the T3-campaign (Ruessink, 1998a). The bed material consisted of well-sorted, fine to medium sand with a median grain size d_{50} of 155, 165, 170 and 180 μm at P1, P2, P3 and P4, respectively.

At all positions, an electromagnetic flowmeter (EMF) and a pressure sensor were mounted on stand-alone tripods at nominal heights z of 0.25 and 2.2 m above the bed, respectively, while the tripods at P2, P3 and P4 were additionally equipped with two Optical Backscatter Sensors (OBSs) at $z = 0.15$ and 0.25 m to measure sediment concentration. Given the absence of OBSs at P1, the flux analysis in this paper is restricted to the remaining three positions. All measurements were sampled for about 35 min per hour at a frequency of 2 Hz. Unfortunately, the tripod at P3 malfunctioned during the largest part of the T4-campaign.

Each OBS-sensor was calibrated in a sediment recirculation tank using sand from its deployment site. The sensor output correlated linearly with the sediment concentration over the range from 0 to 40 kg m^{-3} ($R^2 > 0.99$). In the field, a small (<0.5 kg m^{-3}) offset was encountered for each OBS. Its value was fairly constant during a campaign and could have a positive or negative sign. The origin of the offset is unknown; it may be associated with calibration inaccuracies at very low concentrations. Given the fact that the offset could also be negative, it seems unlikely that it resulted from a natural background concentration of mud or organic particles. In the analysis presented below the offset was simply subtracted from all observations, resulting in a background concentration of 0 kg m^{-3}.

An important element in the analysis of the degree to which the various hydrodynamical processes contribute to the sediment transport is the objective description of the local hydrodynamical conditions. Terms like 'fair weather' and 'storm' do not suffice, because they are subjective and have to be interpreted differently for different depth ranges. Here, the relative wave height, defined as the ratio between the local significant short-wave height H_s and water depth h, was applied. Values of H_s were computed as $4E^{0.5}$, where E is the variance of the free surface elevation in the short-wave frequency band 0.04–0.33 Hz. Time series of the free surface elevation were calculated from the measured pressure time series with a depth correction using linear wave theory. The lower frequency limit of the short-wave frequency band marks the separation with the infragravity band, taken as 0.004–0.04 Hz (Ruessink, 1998a); variance at frequencies >0.33 Hz could not be properly depth-corrected.

The main advantage of using H_s/h as a conditional parameter is its usability as a breaker criterion (see, for example, Osborne and Greenwood, 1992). A combination of extensive visual observations and measurements in the intertidal zone at the Terschelling site revealed that the onset of short-wave breaking occurred at a value of $H_s/h = 0.33$ (Van Enckevort and Reincke, 1996). This value corresponds to the breaking of the highest waves in a wave group. When the breaking intensity increases (i.e., more breaking waves), H_s/h increases until all waves are broken (Thornton and Guza, 1982). The maximum H_s/h value observed by Van Enckevort and Reincke amounted to 0.59. As motivated by Ruessink (1998b), the same H_s/h values marking the onset of breaking and saturation can also be used in the nearshore bar zone.

A wide range of offshore wave conditions was encountered with H_s at the offshore station (i.e., P1) varying between 0.2 and 4.5 m. The significant offshore wave period $T_{1/3}$, calculated with a standard zero-down-crossing technique in the time domain, ranged from 4.0 to 15.5 s. The wave conditions were generally sea-dominated with true swell being limited to only a few occasions. The angle of wave incidence α at P1 had maximum values of up to several tens of degrees to the shore normal. Especially, the more energetic wave events (say, H_s at P1 > 3 m) had an almost shore-normal incidence ($\alpha <\approx 15°$).

The tide was semi-diurnal with neap and spring tidal ranges of about 1.2 and 2.5 m, respectively.

3. Methodology

3.1. Sediment fluxes

Time series of instantaneous concentration c and cross-shore velocity u can be decomposed into a mean (overbar) and oscillating (tilde) component. The net time-averaged sediment flux $\langle uc \rangle$, where averaging is performed over a measurement and is denoted by $\langle\ \rangle$, consists of a mean and oscillating part:

$$\langle uc \rangle = \langle (\bar{u} + \tilde{u})(\bar{c} + \tilde{c}) \rangle = \bar{u}\bar{c} + \langle \tilde{u}\tilde{c} \rangle \quad (1)$$

The first term on the right-hand side of Eq. 1 is the mean-flow-related suspended sediment flux, computed as the product of the time-averaged cross-shore velocity and the time-averaged concentration. The second term is referred to as the wave-related (or oscillatory) flux, which is non-zero when fluctuations in cross-shore velocity and concentration are correlated. The oscillatory component can be subdivided into a high- and low-frequency part, denoted with subscripts h and l, respectively, as defined in Section 2. The time-averaged wave-related flux can now further be expanded as (dropping the tilde in the high- and low-frequency components):

$$\langle \tilde{u}\tilde{c} \rangle = \langle (u_h + u_l)(c_h + c_l) \rangle = \langle u_h c_h \rangle + \langle u_l c_l \rangle \quad (2)$$

The two terms on the right-hand side of Eq. 2 are called the high-frequency and low-frequency sediment flux, respectively. Terms consisting of the product of a high- and low-frequency component were not retained in Eq. 2. These interaction fluxes are very small compared to the other ones because high- (low-) frequency fluctuations in u are, in general, uncorrelated to low- (high-) frequency oscillations in c. Eqs. 1 and 2 can be combined into:

$$\langle uc \rangle = \bar{u}\bar{c} + \langle u_h c_h \rangle + \langle u_l c_l \rangle \quad (3)$$

Positive (negative) values indicate onshore (offshore) fluxes.

For the calculation of the mean-current-related flux at the lower OBS-sensor, the mean flow measured by the EMF was depth-corrected using a simple engineering rule (Van Rijn, 1991):

$$\bar{u}_1 = \bar{u}_2 \left(\frac{z_1}{z_2} \right)^{0.25} \quad (4)$$

where subscripts 1 and 2 denote two different heights above the bed. With $z_1 = 0.15$ m and $z_2 = 0.25$ m, the mean flow at the height of the lower OBS was estimated as 88% of that measured by the EMF. The oscillatory flows were not depth-corrected.

The actual distance of the sensors off the bed during the campaigns is expected to have varied (at least) several centimetres because of ripple dynamics, local erosion or sedimentation near the tripod, or slow settling of the tripod into the bottom. Unfortunately, simultaneous measurements of bed elevation were not available and the precise values of the sensor elevations are thus unknown for each measurement. Therefore, the two OBSs will simply be referred to as the 'lower' and 'upper' sensor in the remainder of this paper. The applied depth correction (Eq. 4) is not greatly (<10%) affected by variations in z_1 and z_2 of the order of several centimetres. The correction value of 88% was thus applied for all measurements. The effect of the instruments and the tripod configuration on the local flow and sediment suspension characteristics is expected to be negligible.

Detailed information on the frequency dependence of the wave-related fluxes can be obtained from cross-spectral analysis. The co-spectrum, that is, the real part of the cross-spectrum, is used to investigate the magnitude and direction of the oscillatory fluxes as a function of frequency (cf. Huntley and Hanes, 1987). The integral of the co-spectrum over the infragravity-frequency and short-wave frequency region are equal to the time-averaged oscillating fluxes (second and third term on the right-hand side of Eq. 3, respectively). The phase-spectrum and the coherence-squared diagram provide information on the phase lags and the (linear) correlation between u and c as a function of frequency, respectively. Cross-spectral estimates were obtained from detrended, tapered and 50%-overlapping data segments with a length of 256 s. The frequency resolution amounted to about 0.004 Hz. The number of degrees of freedom was 39. The 95% confidence level for significant non-zero coherence-squared values amounted to about 0.16.

3.2. Model description

The total (i.e., bedload and suspended load) time-averaged immersed weight sediment transport in the cross-shore direction $\langle i_t \rangle$ can be estimated with the energetics expression of Bailard (1981) as:

$$\langle i_t \rangle = \langle i_b \rangle + \langle i_s \rangle = \rho c_f \frac{\epsilon_b}{\tan\phi}\left[\langle |u_t|^2 u\rangle - \frac{\tan\beta}{\tan\phi}\langle |u_t|^3\rangle\right] + \rho c_f \frac{\epsilon_s}{w}\left[\langle |u_t|^3 u\rangle - \frac{\epsilon_s}{w}\tan\beta\langle |u_t|^5\rangle\right] \quad (5)$$

The first and second term on the right-hand side of Eq. 5 represent the cross-shore bedload and suspended load part of the immersed weight sediment transport, respectively. In Eq. 5, the subscripts b and s denote bedload and suspended load, respectively, ρ = water density, c_f = a drag coefficient, ϵ_b and ϵ_s = efficiency factors, ϕ = angle of repose ($\tan\phi \approx 0.63$), β = local bottom slope, w = sediment fall velocity, u = instantaneous near-bed cross-shore flow, and $|u_t|$ = total instantaneous near-bed velocity vector. The time-averaged terms in Eq. 5 that are proportional to some power of the instantaneous velocity are also referred to as velocity moments. The terms containing $\tan\beta$ represent the downslope transport by gravity. They were neglected in the present analysis because of the gentle slopes at the field site (Fig. 1). This is in line with results from previous model studies (Stive, 1986; Roelvink and Stive, 1989; Thornton et al., 1996; Gallagher et al., 1998), which all suggest that the gravity-driven transport on natural beaches is relatively small. Furthermore, it is our main aim to determine the contribution of the mean and oscillatory flows to the sediment transport.

To examine various transporting mechanisms, the total velocity vector was split into a cross-shore and longshore component (v), each of which was subdivided into a mean (overbar) and an oscillating (tilde) component. The total velocity vector can now be written as:

$$|u_t| = \left[\bar{u}^2 + \tilde{u}^2 + \bar{v}^2 + \tilde{v}^2 + 2(\bar{u}\tilde{u} + \bar{v}\tilde{v})\right]^{0.5} \quad (6)$$

The bedload moment is directly expanded as:

$$\langle |u_t|^2 u\rangle = \langle |\tilde{u}|^2\tilde{u}\rangle + 3\bar{u}^2\langle |\tilde{u}|\rangle + \bar{u}^3 + \bar{v}^2\bar{u} + \ldots \quad (7)$$

A problem in the actual computing of the velocity moments in Eq. 7 is the height above the bed at which the velocity information should be specified. This problem especially concerns the value of the mean flow because of the vertical shear in the near-bed region. In Bailard (1981) the bedload layer has the thickness of a few grain diameters, whereas the thickness of the suspended load layer approximately equals that of the wave bottom boundary layer. Nairn and Southgate (1993) suggested that "the mean or time-averaged velocity applied to the bed load should be that determined for the boundary layer and similarly a velocity at some height above the boundary layer should be used for the suspended load terms in the energetics expression". In practice, the recordings of a near-bed (z in the order of a few decimetres) velocity sensor are applied for the computation of the mean-flow bedload moment (see, for example, Russell et al., 1995; Thornton et al., 1996; Gallagher et al., 1998). Here the mean flow in the bedload equation was taken as the mean flow at the top of the bottom boundary layer, $\bar{u}_\delta$, estimated with Eq. 4. The thickness of the wave bottom boundary layer δ was computed as (Van Rijn, 1993):

$$\delta = 0.072\,\hat{A}_\delta(\hat{A}_\delta/k_{s,w})^{-0.25} \quad (8)$$

In Eq. 8, $k_{s,w}$ is the wave-related bottom roughness, set to a constant value of 0.01 m (Van Rijn, 1993), and $\hat{A}_\delta$ is the near-bed peak orbital excursion, computed here with linear wave theory. It is stressed that the findings of the relative importance of bedload versus suspended load were not profoundly affected by the choice of $\bar{u}$ in the bedload expression. The oscillatory bedload components were calculated with the measured time series at $z = 0.25$ m, because the depth variations of the oscillating flow near the bed are theoretically negligibly small.

Ruessink (1998a) extensively analysed all ten moments on the right-hand side of Eq. 7 at all four measuring stations and concluded that:

$$\langle |u_t|^2 u\rangle \simeq \langle |\tilde{u}|^2\tilde{u}\rangle + 3\bar{u}_\delta\langle |\tilde{u}|^2\rangle \quad (9)$$

This implies that all longshore flow components can be discarded from the analysis.

The suspended load moment cannot be directly expanded and has to be approximated by series expansions. If, consistent with the bedload findings, longshore flow components are neglected and the oscillatory motions are dominant over the mean flow,

the suspended load moment can be expanded in a binomial series (see Bowen, 1980; Roelvink and Stive, 1989):

$$\langle |u_t|^3 u \rangle \simeq \langle |\tilde{u}|^3 \tilde{u} \rangle + 4\bar{u}\langle |\tilde{u}|^3 \rangle + 6\bar{u}^2 \langle \tilde{u}|\tilde{u}| \rangle + \ldots \quad (10)$$

Only the largest two moments on the right-hand side of this equation (first and second terms) were retained.

By splitting the oscillatory flow into a high- and low-frequency component (subscripts h and l, respectively) and by assuming $u_h \gg u_l$ and u_h to be uncorrelated to $|u_l|^2$ and $|u_l|^3$, Eqs. 9 and 10 can be rewritten into (see Roelvink and Stive, 1989):

$$\langle |u_t|^2 u \rangle \simeq \langle |u_h|^2 u_h \rangle + 3\langle |u_h|^2 u_l \rangle + 3\bar{u}_\delta \langle |u_h|^2 \rangle \quad (11)$$

and:

$$\langle |u_t|^3 u \rangle \simeq \langle |u_h|^3 u_h \rangle + 4\langle |u_h|^3 u_l \rangle + 4\bar{u}\langle |u_h|^3 \rangle \quad (12)$$

respectively. The afore-mentioned requirements to derive Eqs. 11 and 12 were met for the range of conditions presented in this paper. As can be deduced from Eqs. 11 and 12, the stirring of sand is proportional to the high-frequency cross-shore orbital flow to the power of two in the bedload and three in the suspended load. Hereafter the three terms on the right-hand side of Eqs. 11 and 12 are referred to as the high-frequency, low-frequency and mean-flow velocity moments, respectively. The high-frequency moments are non-zero when the stirring terms $|u_h|^2$ and $|u_h|^3$ are systematically related to u_h. This is the case for short-wave asymmetry about the horizontal plane ('skewness'), caused by non-linearities. It results, in general, in positive (= onshore direction) values. The low-frequency moments attain a non-zero value if the predicted sediment stirring is systematically coupled to u_l. Such a coupling exists, for example, in case of group-bound long waves, which results in negative (= offshore direction) values as the phase shift between the wave envelope and the forced infragravity waves amounts to approximately 180 degrees (Longuet-Higgins and Stewart, 1962; Larsen, 1982; Ruessink, 1998c). The mean-flow moments correspond to the advective transport by a mean cross-shore flow. Clearly, the direction of this part of the total load equals that of the flow.

The velocity time series measured at $z = 0.25$ m were used to calculate the suspended load moments. In fact, this approach assumes that the layer in which most of the suspended load occurs has a reasonably uniform vertical velocity profile, with here $z = 0.25$ m being the reference level. As described earlier, this approach is justified for the oscillatory moments; it is less clear for the value of the mean-flow moments. Of special interest in this respect is the work by Thornton et al. (1996) and Gallagher et al. (1998). These authors predicted cross-shore gradients in sediment transport over a small nearshore bar with Bailard's (1981) energetics expression, and compared the predicted morphological changes with the measured bar behaviour. They found the suspended load to dominate over the bedload; the value of the mean flow they applied was measured at several decimetres above the bed. The modelled and observed bar development agreed reasonably well, which suggests that velocity recordings at several decimetres above the bed can indeed be considered as reference values for suspended sediment transport calculations with the energetics model of Bailard (1981).

Values have to be specified for ϵ_b, ϵ_s and w in order to know more about the relative importance of the bedload with respect to the suspended load. The reader is referred to Nairn and Southgate (1993) for an extensive overview of the calibration of the efficiency factors. Here, ϵ_b and ϵ_s were set to 0.21 and 0.025, respectively. These values are the same as or close to those used by other researchers (Bailard, 1981; Stive, 1986; Nairn and Southgate, 1993; Thornton et al., 1996; among others). The applied median sediment fall velocities at P1, P2, P3 and P4 were 15.1, 17.7, 19.7 and 20.5 mm/s, respectively. It is stressed that the energetics approach is used here as a qualitative tool; besides for the investigation on the importance of bedload and suspended load to the total load, the absolute magnitudes of the transports are not considered.

All calculated moments were binned corresponding to $H_s/h \pm 0.01$, that is, categorised into H_s/h groups with a width of 0.02. In this way, the generality of all our measurements is highlighted. The total number of measurements used in the model computations presented below amounted to 2420, 2096, 1326 and 1408 at P1, P2, P3 and P4, respectively.

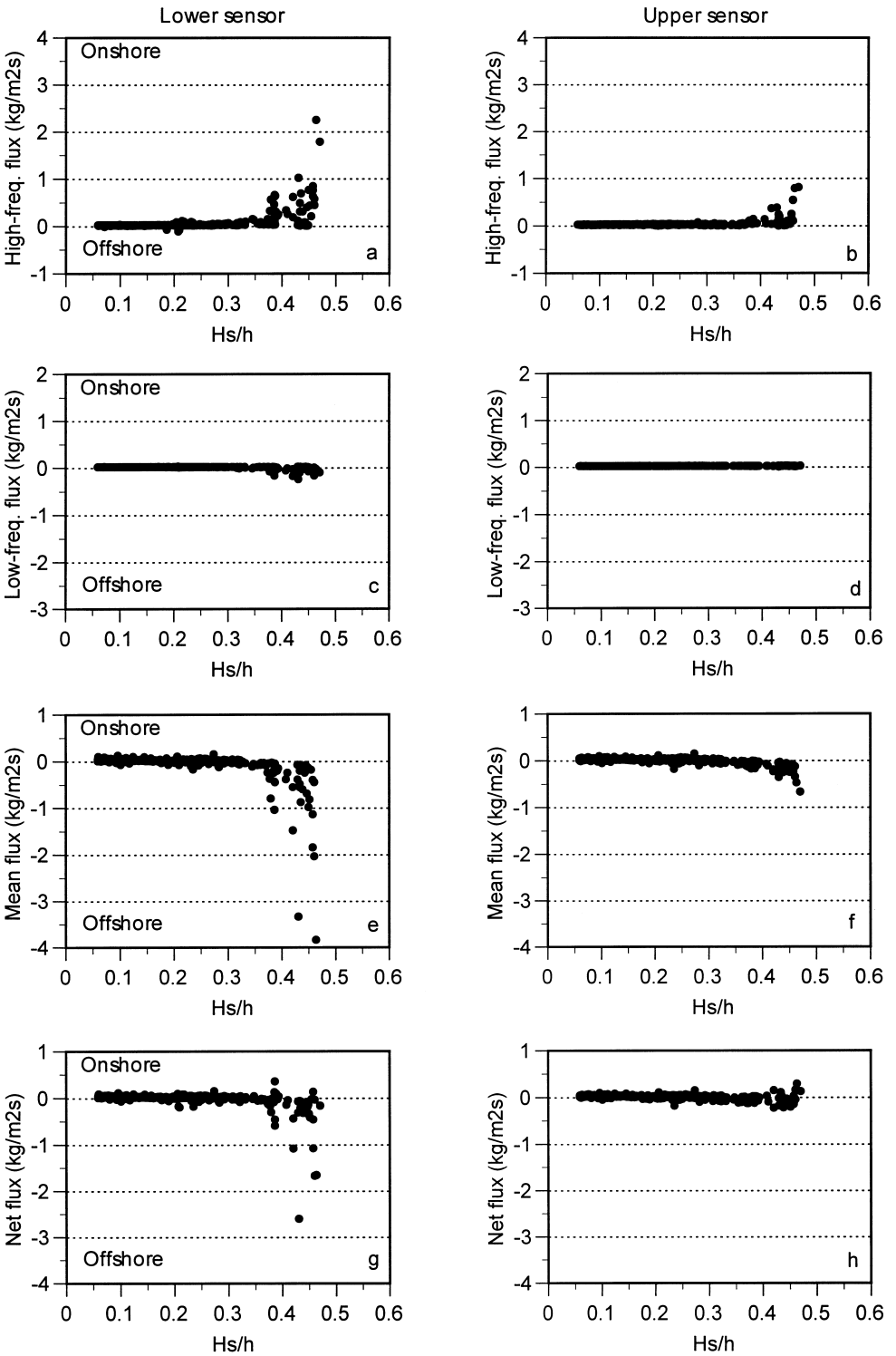

Fig. 2. Measured (a, b) high-frequency, (c, d) low-frequency, (e, f) mean and (g, h) net fluxes at the lower OBS (left column) and the upper OBS (right column) as a function of the local relative wave height H_s/h at P2 (T4-campaign).

4. Measured sediment fluxes

4.1. P2 (seaward side of outer bar, $h \approx 5.5$ m)

The values of the high-frequency, low-frequency, mean and net suspended sediment fluxes at P2 are plotted in Fig. 2 as a function of H_s/h. These values were based on the T4-campaign because this campaign spanned the widest range of H_s/h conditions at this position. The flux measurements performed during the T2- and T3-campaign resulted in approximately the same magnitudes and trends as shown in Fig. 2 for the T4-campaign. Therefore they are not shown separately. As can be seen, the oscillatory and mean fluxes were only non-zero for situations with $H_s/h > 0.3 - 0.35$ at the lower sensor and $H_s/h > 0.35 - 0.4$ at the upper sensor, in other words, during situations when P2 experienced surf zone conditions. The high-frequency fluxes were onshore directed and, at a first glance, of roughly equal magnitude to the current related ones (for instance, compare Fig. 2a and 2e), which were of opposite sign (seaward directed). The low-frequency fluxes were offshore directed as well, but were considerably smaller than the other fluxes, especially at the upper sensor. The high-frequency and mean flux increased rapidly with H_s/h, whereas the low-frequency flux remained about constant. All fluxes diminished with elevation for a specific H_s/h value. As can be seen in Fig. 2, the scatter around the above-mentioned general H_s/h dependencies was quite considerable. This is likely due to varying distances between the bed and the instruments during the campaign. Even a small change in instrument position relative to the bed may cause a significant change in the magnitude of the current- and wave-related transports, because gradients in the mean concentration and, presumably, the oscillations around it are very high close to the bed. In addition, changes in the phase relationship between the high-frequency cross-shore fluid motion and concentration may have attributed to the scatter in the high-frequency transports. Such phase relationships are profoundly influenced by bedforms, as shown by, for instance, Osborne and Greenwood (1992) on a natural barred beach. The observed variability in Fig. 2a and b seems to suggest that bedform variability indeed occurred. Unfortunately, direct bedform observations were not made during the measurements. The bedform classification scheme of Van Rijn (1993) suggests that the possible bedforms in the nearshore zone of Terschelling are mainly wave-dominated. In case of bedforms under waves, Van Rijn (1993) proposed that ripple characteristics are related to the mobility parameter ψ, which reads as:

$$\psi = \frac{\hat{U}_\delta^2}{(s-1)gd_{50}} \tag{13}$$

In Eq. 13, $\hat{U}_\delta$ is the peak near-bed orbital velocity, s is the specific density and g is the gravitational acceleration. A transition from a rippled to a plane bed (sheetflow conditions) is predicted at $\psi = 250$. With $d_{50} = 165$ μm this corresponds to $\hat{U}_\delta \sim 0.8$ m/s. With a typical period of 7 s and a water depth of 5.5 m, this results in $H_s = 1.4$ m (linear wave theory) and $H_s/h \sim 0.25$. This suggests that all measurements with significant non-zero fluxes were obtained under sheetflow conditions and that changes in sensor elevation may be the main cause of the variability in the measured fluxes. Despite this, it has to be kept in mind that there is no generally accepted formulation for the predictions of bedforms under natural (wave) conditions and that errors associated with the predictions may be considerable.

Although the net fluxes were still offshore directed (Fig. 2g and h), especially at the lower sensor, they were smaller than the mean fluxes. Clearly, models that predict transport by mean flows alone are inadequate. The small net fluxes demonstrate that the cross-shore sediment transport at P2 (at least, at the elevations above the bed shown here) was a delicate balance between contributions by mean currents and by short and long waves.

All reliable measurements of the T2-, T3-, and T4-campaigns were subjected to cross-spectral analysis to improve the understanding of the observed trends of the oscillatory fluxes with H_s/h. In general, the coherence between the oscillatory components of u and c were insignificant or very poor (coherence values of up to 0.2) at all frequencies for $H_s/h < 0.29$ and $H_s/h < 0.35$ at the lower and upper sensor, respectively. Accordingly, the wave-related fluxes were about zero in these situations. It implies that the sand was suspended neither on the

time scale of the individual short waves nor on that of the infragravity waves (e.g., group enhanced).

The cross-spectral results for measurements with non-zero oscillatory fluxes the more energetic situations up to $H_s/h \approx 0.45$ are described on the basis of a representative measurement ($H_s/h = 0.39$). Fig. 3 presents the first 6 min of the detrended cross-shore velocity and concentration time series of this selected example. The thick line in Fig. 3a is the low-frequency part of u. It has all the characteristics of a bound long wave, viz. a trough under the high waves (e.g., $t = 220$ to 260 s, where t is time) and a crest under the low waves (e.g., $t = 40$ to 70 s). Ruessink (1998c) used bispectral analysis to show that at P2 approximately 40 to 80% of the total infragravity energy is locally bound to the wave groups for $H_s/h \approx 0.4$. It is clear that the observed sediment concentrations at the lower sensor showed a markedly intermittent pattern in which high-frequency oscillations in c closely corresponded to those in u. The sediment resuspension was strongly enhanced during the succession of several high waves (e.g., from $t = 220$ to 260 s). Note that the number of concentration peaks during the passage of a wave group approximately equalled the number of waves; in other words, the sediment was stirred once per wave cycle. Comparable results have been presented for non-breaking con-

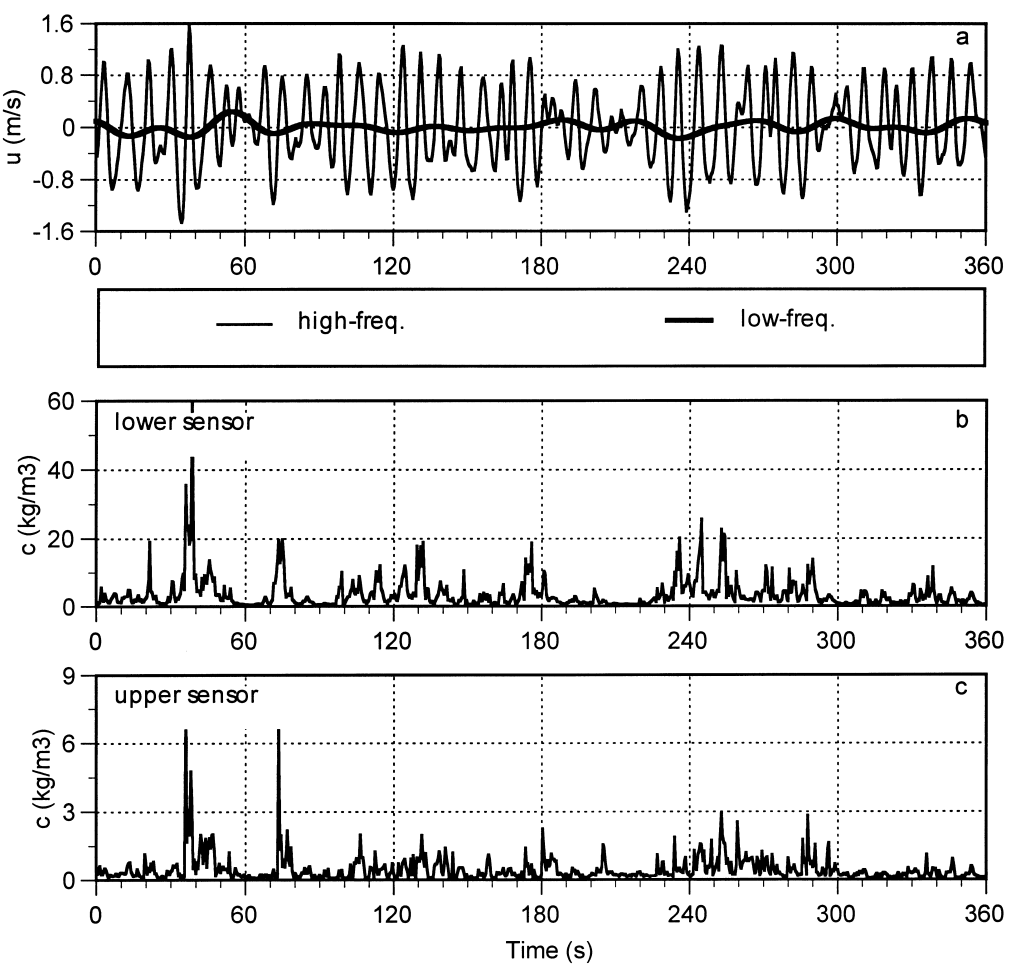

Fig. 3. Representative example of intraburst time series of: (a) cross-shore velocity, (b) suspended sediment concentration at the lower OBS, and (c) suspended sediment concentration at the upper OBS during situations with a relative wave height between ≈0.29 and 0.45 (P2; $H_s/h = 0.39$).

ditions by, for instance, Hanes and Huntley (1986), Hanes (1990, 1991) and Osborne and Greenwood (1992). The same resuspension features were also visible at the upper sensor, although especially the group-enhanced stirring was less pronounced.

The frequency-domain analysis of the time series in Fig. 3 is presented in Fig. 4. The peak frequency f_p of the cross-shore velocity spectrum, plotted in Fig. 4a, was about 0.12 Hz ($T_p \approx 8$ s). The concentration spectrum of the lower sensor had a well-developed peak associated with the incident wave field; at the upper sensor this peak was less distinct (Fig. 4a). Note that if the sediment had been suspended twice per wave cycle, during both the onshore and offshore phase of the cross-shore fluid motion, the spectrum would have shown a peak at 2

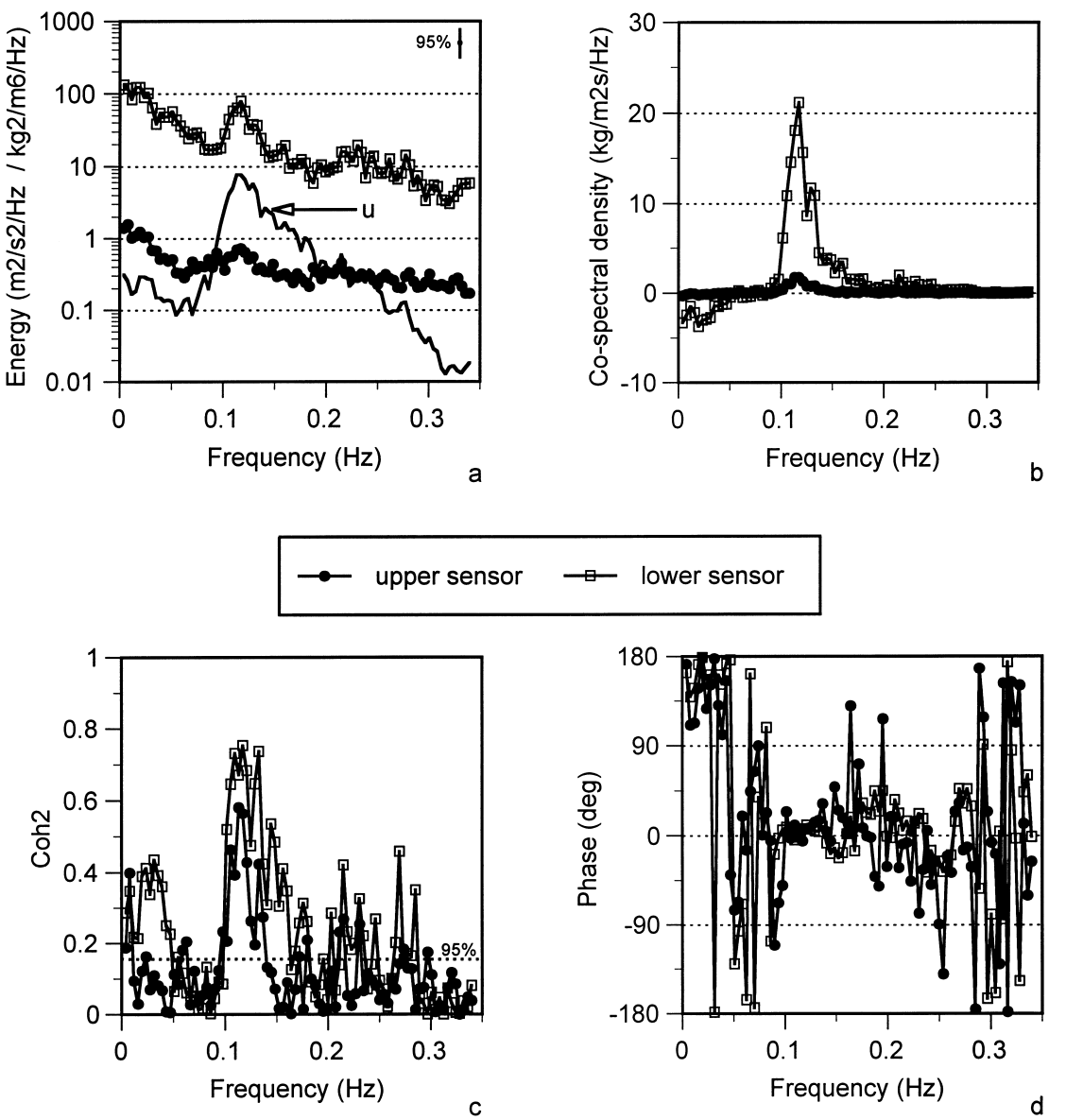

Fig. 4. Frequency-domain analysis of time series shown in Fig. 3: (a) variance density spectra, (b) co-spectra, (c) coherence-squared diagrams, and (d) phase diagrams.

f_p. The remaining parts of the concentration spectra were rather featureless and tended to increase gently to lower frequencies. Also notable is the rapid reduction in concentration variance at all frequencies with elevation. The co-spectrum at the lower sensor revealed a relatively large positive peak at f_p (= onshore transport) and a smaller negative peak at infragravity frequencies (Fig. 4b). As such, the co-spectrum closely resembles those published by others for measurements under non-breaking conditions (e.g., Huntley and Hanes, 1987; Beach and Sternberg, 1991; Osborne and Greenwood, 1992; Aagaard and Greenwood, 1994). The co-spectrum at the upper sensor possessed similar features, although its densities were considerably smaller compared to those at the lower sensor. The coherence between the oscillatory cross-shore velocities and concentrations was significant around f_p and at infragravity frequencies (Fig. 4c). The smaller (even insignificant) coherence values in the infragravity region at the upper sensor indicate that the low-frequency oscillations in c were less well related to the group-enhanced stirring at the upper than at the lower sensor. This was also noted from the visual inspection of the time series (Fig. 3). The oscillations in the short-wave frequency band were almost in phase (Fig. 4d), which means that the intermittent concentration events mainly occurred during the onshore phase of the orbital motion. At the infragravity frequencies, the phases were about 120 to 180 degrees (or, alternatively, -240 to -180 degrees), implying that the low-frequency concentration oscillations lagged the wave groups by 0 to 60 degrees. However, the wave-group-induced stirring still coincided with the passage of a bound long-wave trough (e.g., compare Fig. 3a and c), resulting in an offshore directed transport (Fig. 4b). Transformed into the time-domain, the infragravity concentration oscillations lagged a measure of the wave envelope by about 0 to $1T_p$. As can be deduced from Fig. 4d, lags between the concentration signals at both sensors around f_p and at infragravity frequencies were minimal. The smaller wave-related fluxes at the upper sensor were thus related to the rapid reduction in concentration variance with height and not to increasing phase differences.

During the most energetic conditions encountered ($H_s/h > \approx 0.45$) the sediment at P2 was still resuspended on the time scale of the individual waves, but the group-enhanced modulation was less clear. The high-frequency region of the co-spectra showed similar features as shown in Fig. 4b, whereas at infragravity frequencies both onshore and offshore transports were measured. Integration of the co-spectra over the infragravity-frequency band, however, still revealed a negative transport. Even though breaking was intense during these conditions, the wave-related flux was strongly dominated by the onshore-directed transport associated with the incident waves (e.g., compare Fig. 2a and c). The destruction of the wave groups by breaking, and as a consequence the less distinct group-enhanced sediment stirring, may explain why the low-frequencies flux did not increase with H_s/h, as previously noted in Fig. 2.

The mean currents at P2 for $H_s/h < \approx 0.30$ were, in general, of the order of a few centimetres per second and could have both a positive or negative sign. These magnitudes are close to (or, probably, even within) the measurement accuracy of the EMF; therefore, the mean fluxes under these conditions were not further considered. In addition, the mean concentrations were relatively small as well (smaller than about 0.5 to 1 kg m^{-3}). Under breaking conditions, the mean flows were offshore directed and generally increased with H_s/h. The observed intensification of the mean cross-shore flows with breaking, which is also produced (at least qualitatively) by simple equations based on the conservation of mass under breaking waves (e.g., Van Rijn, 1990), as well as their temporal consistency suggest that these flows were undertows. Maximum values of up to -0.35 m/s at $z = 0.25$ m were observed. The lower fluxes at the upper sensor reflect the high vertical gradients in mean concentration.

The importance of a flux to the cross-shore suspended sediment transport can be expressed as its relative contribution to the gross sediment transport. The terms 'relative' and 'gross' imply that the direction (sign) of the fluxes is neglected; only the absolute values of the fluxes are considered. As an example, the relative contribution of the high-frequency flux to the gross suspended flux reads as:

$$\frac{|\langle u_h c_h \rangle|}{|\langle u_h c_h \rangle| + |\langle u_l c_l \rangle| + |\bar{u}\bar{c}|} \tag{14}$$

Fig. 5 shows the relative magnitude of the wave- and current-related fluxes to the gross flux for

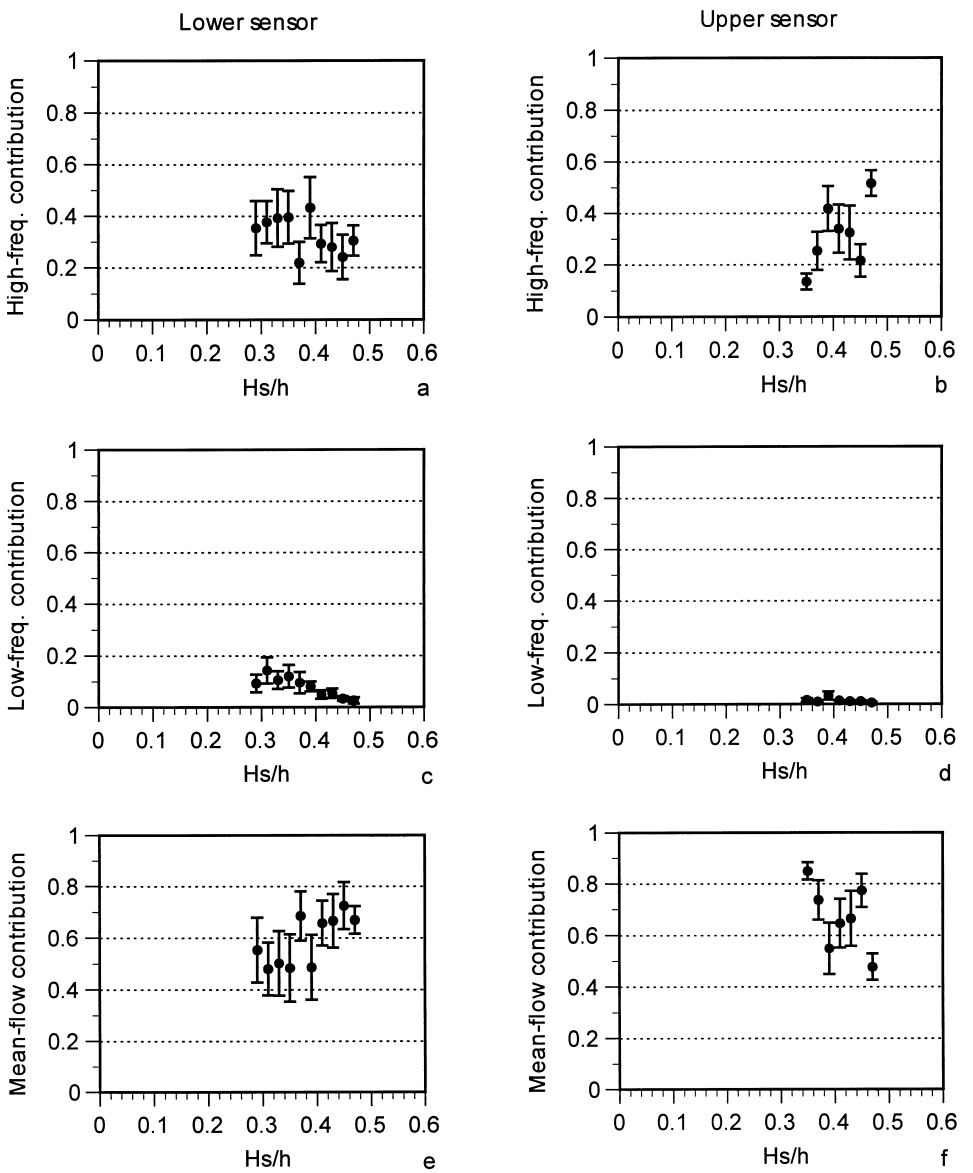

Fig. 5. The relative contribution of (a, b) short waves, (c, d) infragravity waves, and (e, f) mean flows to the gross suspended sediment flux at the lower OBS (left column) and the upper OBS (right column) as a function of the local relative wave height H_s/h at P2 (T4-campaign). The vertical line through each class-mean value is the standard deviation.

$H_s/h \geq 0.29$ and $H_s/h \geq 0.35$ at the lower and upper sensor, respectively. The results were binned corresponding to $H_s/h \pm 0.01$ to illustrate the general trends more clearly. The vertical line through each symbol (mean value) denotes the standard deviation. At both sensors the mean flow and short waves dominated the net flux with relative mean contributions of 0.5–0.8 and 0.2–0.5, respectively (Fig. 5a, b, e and f). At the lower sensor, the infragravity-induced flux contributed about 15% to the gross flux at the onset of breaking (Fig. 5c); at the upper sensor, the low-frequency contribution was almost nil (Fig. 5d). The orbital flux was increasingly dominated by the short-wave motions with increasing breaking inten-

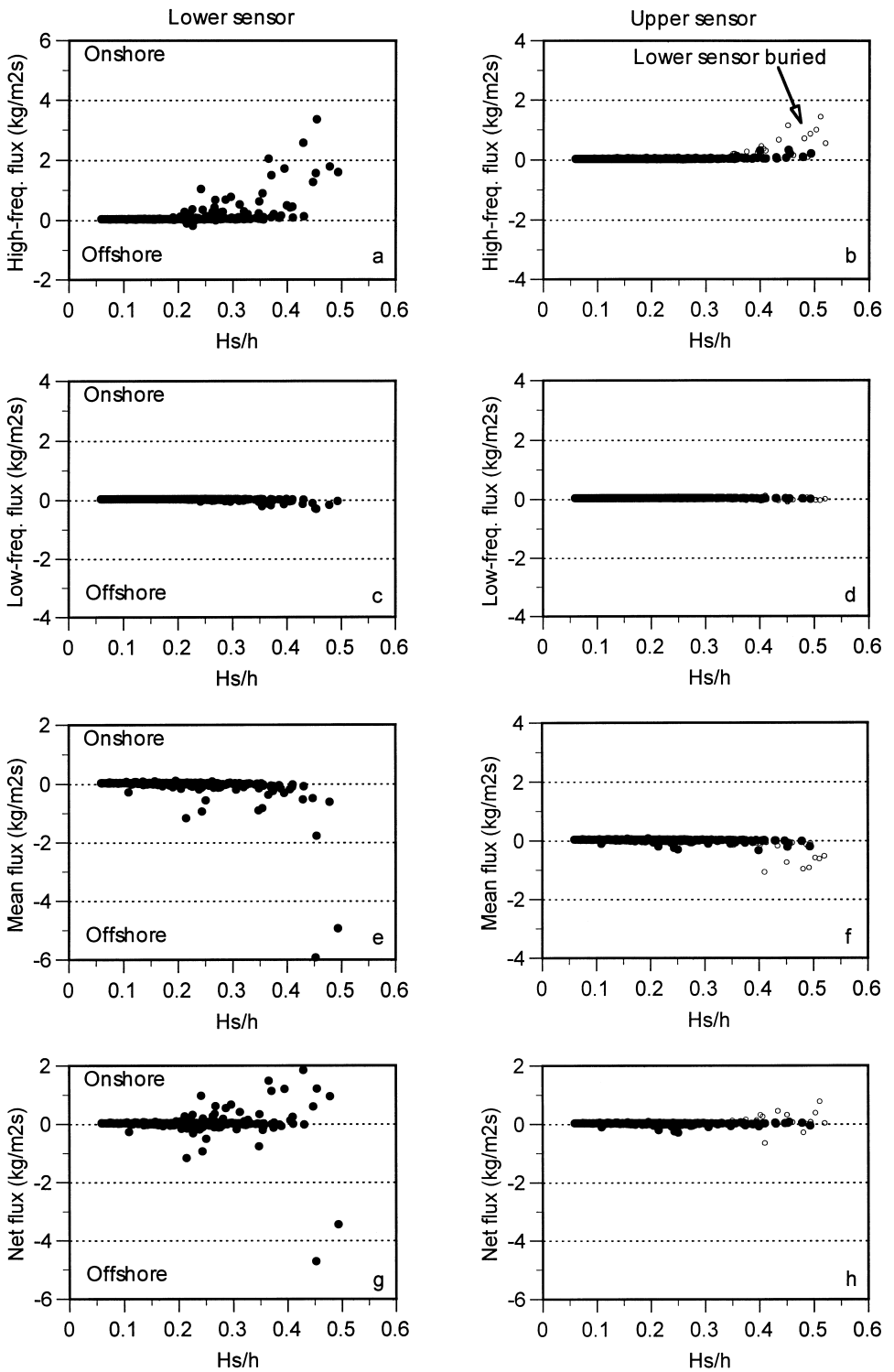

Fig. 6. Measured (a, b) high-frequency, (c, d) low-frequency, (e, f) mean and (g, h) net fluxes at the lower OBS (left column) and at the upper OBS (right column) as a function of the local relative wave height H_s/h at P3 (T3-campaign).

sity (growing H_s/h). Accordingly, the relative contribution of the infragravity flux diminished during more energetic conditions.

4.2. P3 (seaward side of middle bar, $h \approx 3.5$ m)

The values of the high-frequency, low-frequency, mean and net fluxes at P3, measured during the T3-campaign, are plotted versus H_s/h in Fig. 6. Twenty values calculated for the lower sensor had to be omitted from these graphs and the subsequent analysis because of a high number of overflow values. The corresponding H_s/h values varied between 0.34 and 0.52. Probably, the lower sensor was extremely close to or even within the bed during these measurements. The observed transports at the upper sensor during the 'overflow'-bursts were given a different symbol (open circle) to mark them off from the other measurements. As can be seen, these fluxes were, on average, significantly larger than those at the same H_s/h values observed during other parts of the campaign. Thus, the distance between the sensors at P3 and the bed may have varied considerably during the T3-campaign. The remaining fluxes exhibited similar trends with the relative wave height as described previously for P2 (Fig. 2). They differed, however, in detail. For instance, oscillatory fluxes at the lower sensor were already non-zero for $H_s/h > 0.2$. Visual inspection of the corresponding time series as well as cross-spectral analysis confirmed that the sediment was actually resuspended on a short-wave and group scale. However, these wave-related transports were measured only several hours after the 'overflow'-bursts, with the lower OBS probably still at a small distance from the bed. In contrast, measurements with H_s/h values of 0.2–0.3 performed shortly after the onset of the campaign and with the OBSs likely positioned close to their 'nominal' tripod heights (i.e., $z = 0.15$ m and $z = 0.25$ m) revealed only zero high- and low-frequency fluxes, similar to the observations at P2 (Fig. 2). Another difference concerned the few relatively large negative mean fluxes during non-breaking conditions (Fig. 6e; $H_s/h = 0.2$ to 0.25). During these measurements the sediment was advected by strong (up to -0.4 m/s) offshore flows, whose time duration was often limited to a single hour. The origin of these currents is not fully understood; they might have been rip currents because of the observed channel through the bar crest close to the measurement section (see Section 2).

The magnitude of the seaward-directed mean fluxes approximately equalled those of the onshore (total) oscillating fluxes, causing the net flux to have no clear preferential direction with H_s/h (Fig. 6g and h). On the whole, it is fair to say that, just as at P2, the net flux is a subtle balance between contributions made by mean flows and low- and high-frequency waves.

The low-frequency fluxes measured during the T2-campaign were comparable to those of the T3-campaign. In contrast, markedly different trends were observed for the high-frequency and mean fluxes. The short-wave transports at both the lower and upper sensor were offshore directed during a single storm event with H_s at P1 reaching maximum values of 2.5 m, whereas these fluxes had positive values during the remaining part of the campaign. The reverse high-frequency fluxes were caused by lags of over 90° between u_h and c_h, causing c_h to peak during the offshore flow phase. It is stressed here that the offshore fluxes were restricted to this single storm event; phases between u_h and c_h were close to 0° during all other measurements with comparable H_s/h values. The bedform predictions with Van Rijn's (1993) model, see Eq. 13, for the deviating storm event resulted in sheetflow conditions, which was also found for all other storm events with comparable H_s/h values. During the early stages of the T2-campaign, onshore directed cross-shore currents of 0.1–0.2 m/s were measured mainly during low-water bursts with, presumably, an intense wave breaking at the middle bar crest shoreward of P3. In a few cases such currents were also measured when waves were (partially) breaking at P3 itself ($H_s/h > 0.33$) and a wave-driven offshore directed undertow would have been expected. The origin of these onshore flows is unknown; they were not observed during the latter part of the T2-campaign nor during the T3-campaign, even during similar H_s/h conditions.

The relative contributions of the high- and low-frequency waves as well as of the mean flow to the gross sediment transport at P3 (T3-campaign) are plotted versus H_s/h in Fig. 7. Similar to Fig. 5, only the results for $H_s/h \geq 0.29$ (lower sensor) and $H_s/h \geq 0.35$ (upper sensor) are shown, binned ac-

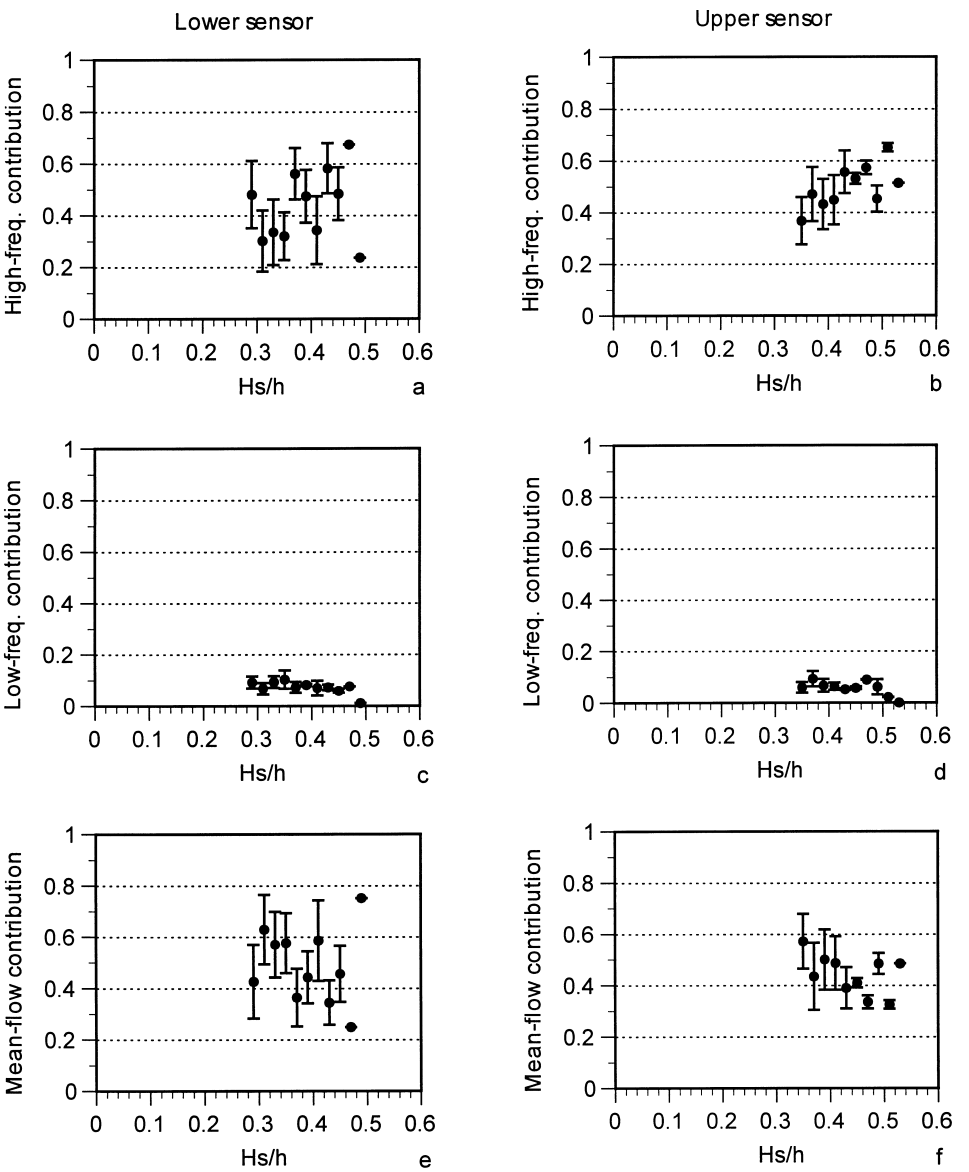

Fig. 7. The relative contribution of (a, b) short waves, (c, d) infragravity waves, and (e, f) mean flows to the gross suspended sediment flux at the lower OBS (left column) and the upper OBS (right column) as a function of the local relative wave height H_s/h at P3 (T3-campaign). The vertical line through each class-mean value is the standard deviation.

cording to $H_s/h \pm 0.01$. The findings for P3 were comparable to those at P2 (Fig. 5), although the short-wave flux tended to be slightly more important (0.3–0.7) than at P2 (0.2–0.5). The larger low-frequency contributions at the upper sensor (compare to Fig. 5d) were likely due to the decrease in distance between the sensor and the bed for the most energetic conditions encountered (note: in Fig. 6 most values for $H_s/h > 0.4$ were marked off with an open circle).

4.3. P4 (middle trough, $h \approx 5.5$ m)

Fig. 8 shows the observed values of the high-frequency, low-frequency, mean-flow and net fluxes at

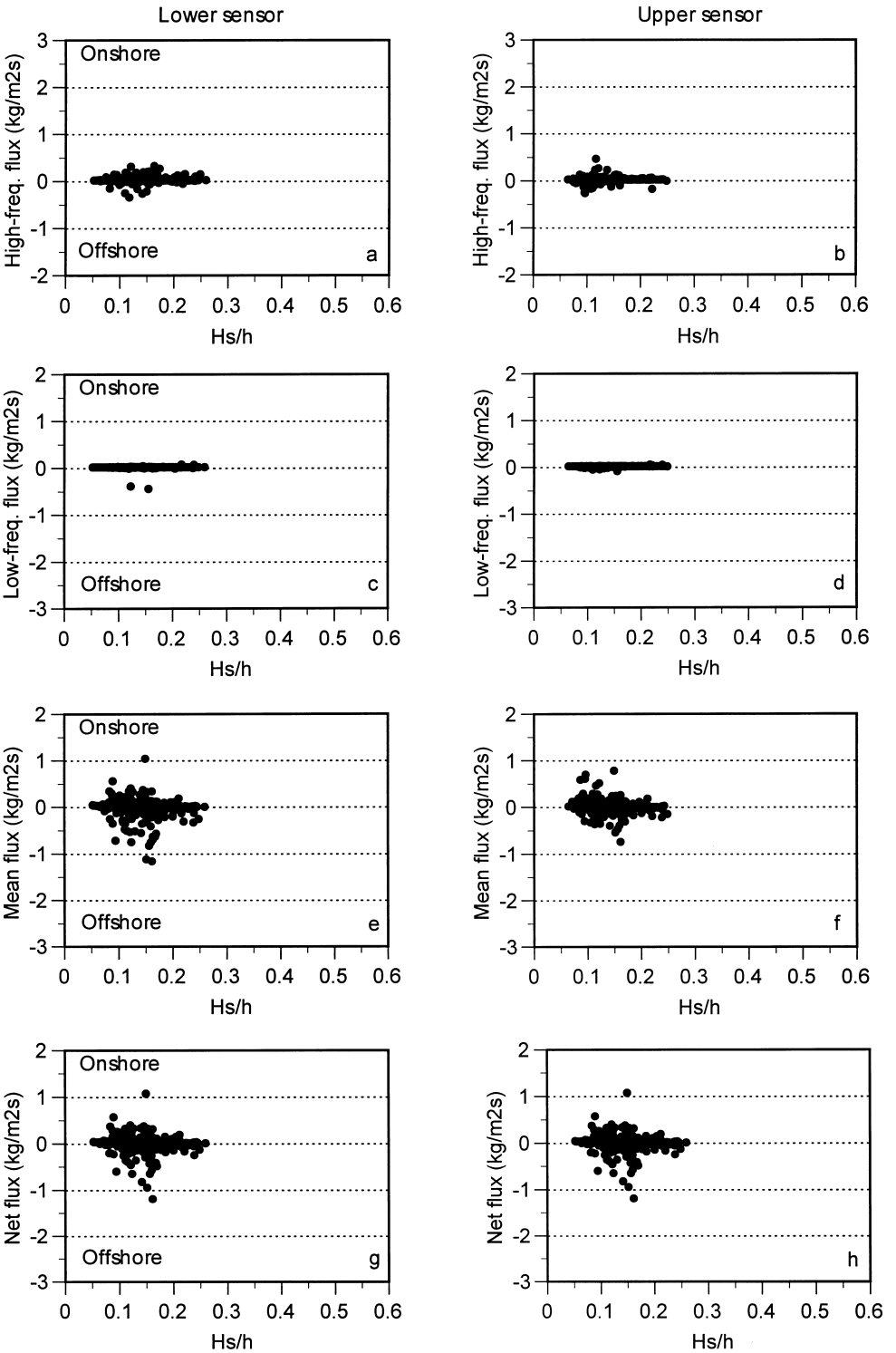

Fig. 8. Measured (a, b) high-frequency, (c, d) low-frequency, (e, f) mean, and (g, h) net fluxes at the lower OBS (left column) and at the upper OBS (right column) as a function of the local relative wave height H_s/h at P4 (T2-campaign).

P4, measured during the T2-campaign, as a function of H_s/h. Comparable results were obtained from the T3- and T4-campaign (not shown). It is quite clear from the H_s/h range in Fig. 8 that the middle bar sheltered P4 from strong wave action (see Fig. 1), as H_s/h did not reach values above $\approx$0.3. Neither the wave-related nor the current-induced flux were related to H_s/h in a systematic way: the measured transports were scattered around the x-axis. Recall that the majority of the non-zero oscillating fluxes at P2 and P3 took place at larger H_s/h values than observed at P4. Although the sediment was occasionally resuspended on the time scale of the individual waves (especially during high-water bursts with minor or no wave breaking at the middle bar), the coherence between the oscillating components of the cross-shore fluid motion and sediment concentration was insignificant or very poor in both the short-wave and infragravity frequency band. This resulted in about zero values of the wave-related fluxes. The net particle flux was, therefore, dominated by the mean flux. It has, however, to be kept in mind that the cross-shore flows at P4 were, on average, very weak ($\approx \pm 0.03$ m/s), rarely reaching values of up to ± 0.15 m/s. Therefore the measured mean fluxes cannot be considered reliable.

4.4. Discussion

As already indicated in Section 1, the findings of this section have to be considered with care. As the exact heights of the sensors above the bed were unknown, the observed general H_s/h dependence of the fluxes can only be regarded as tentative. In addition, the relative contribution of incident waves, infragravity motions, and steady flows, as shown in Figs. 5 and 7, are not necessarily representative of the depth-averaged fluxes. Especially, the lack of observations within a few centimetres above the bed may be unfortunate. For instance, Huntley and Hanes (1987) showed that the depth-averaged net flux was mainly caused by the onshore directed oscillatory flux within 5 cm off the bed, despite the dominance of the offshore directed mean flux at larger heights in the water column. The importance of near-bed measurements to both the magnitude and direction of the net depth-averaged transport was also discussed for field conditions by Ogston and Sternberg (1995). Furthermore, the bedload, that is, the sediment transport taking place very close to the bed, in a thin layer with a thickness of a few millimetres to several centimetres at most, has not been considered at all. These problems will be further addressed with the results of the energetics-based modelling presented in the next section.

5. Energetics-based sediment transport modelling

5.1. The H_s/h dependency of velocity moments

The importance of the bedload transport by a specific process can be expressed as the ratio of the bedload to its total (i.e., bedload and suspended load) transport. For instance, for infragravity waves this ratio reads as:

$$\frac{\frac{\rho c_f \epsilon_b}{\tan\phi}\left[3\langle|u_h|^2 u_l\rangle\right]}{\frac{\rho c_f \epsilon_b}{\tan\phi}\left[3\langle|u_h|^2 u_l\rangle\right] + \frac{\rho c_f \epsilon_s}{w}\left[4\langle|u_h|^3 u_l\rangle\right]} \tag{15}$$

The values of the relative contribution of the bedload to the total load due to short waves, infragravity waves and mean flow at P2 are shown in Fig. 9. The findings at the other positions were virtually identical and are therefore not presented separately. As can be seen for each transporting mechanism, the bedload and suspended load were of comparable magnitude during low-energy conditions ($H_s/h < 0.11$). With increasing relative wave height the suspended load predominated progressively over the bedload. This is not surprising given the fine-grained material at the Terschelling site, and conforms with earlier model studies (e.g., Stive, 1986; Wright et al., 1991; Thornton et al., 1996; Gallagher et al., 1998). Under breaking conditions the suspended load was predicted to be about ten times as large as the bedload (Fig. 9). For this reason, attention is focussed on the suspended load terms in the following.

The fourth-order high-frequency, low-frequency and mean-flow moments, as well as their sum (hereafter referred to as the net moment), are plotted versus H_s/h in Figs. 10–13 for P1, P2, P3 and P4, respectively. At P1, P2 and P3 the high-frequency terms showed characteristic positive values and increased rapidly with H_s/h. The infragravity-induced

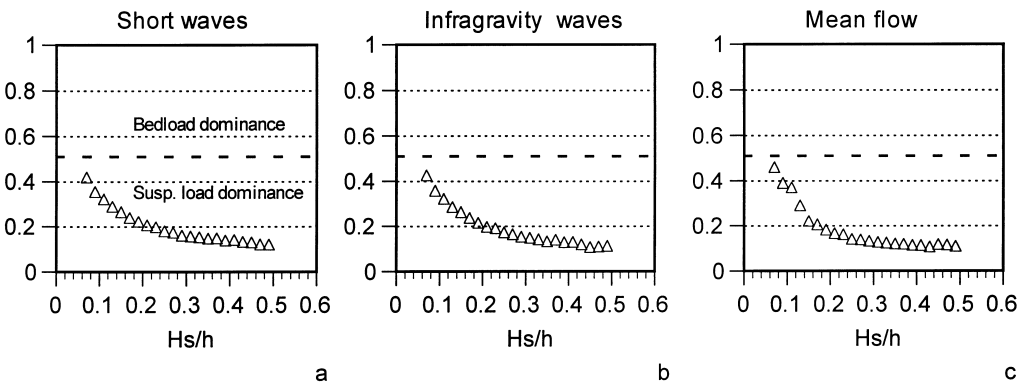

Fig. 9. The relative contribution of bedload to the total load at P2 due to: (a) short waves, (b) infragravity waves, and (c) mean flow. The horizontal dashed line in each graph indicates equal bedload and suspended load contributions.

moments were, as expected, negative, related to the systematic concurrence of high values of $|u_h|^3$ and bound long-wave troughs. At P1 they grew far less rapidly in magnitude with H_s/h than the short-wave asymmetry term and remained about constant with increasing H_s/h for $H_s/h > 0.33$ at P2 and P3. Obviously, the total oscillating suspended transport was onshore directed. The average mean-flow moments indicated onshore and offshore transports of a very small magnitude for situations with H_s/h val-

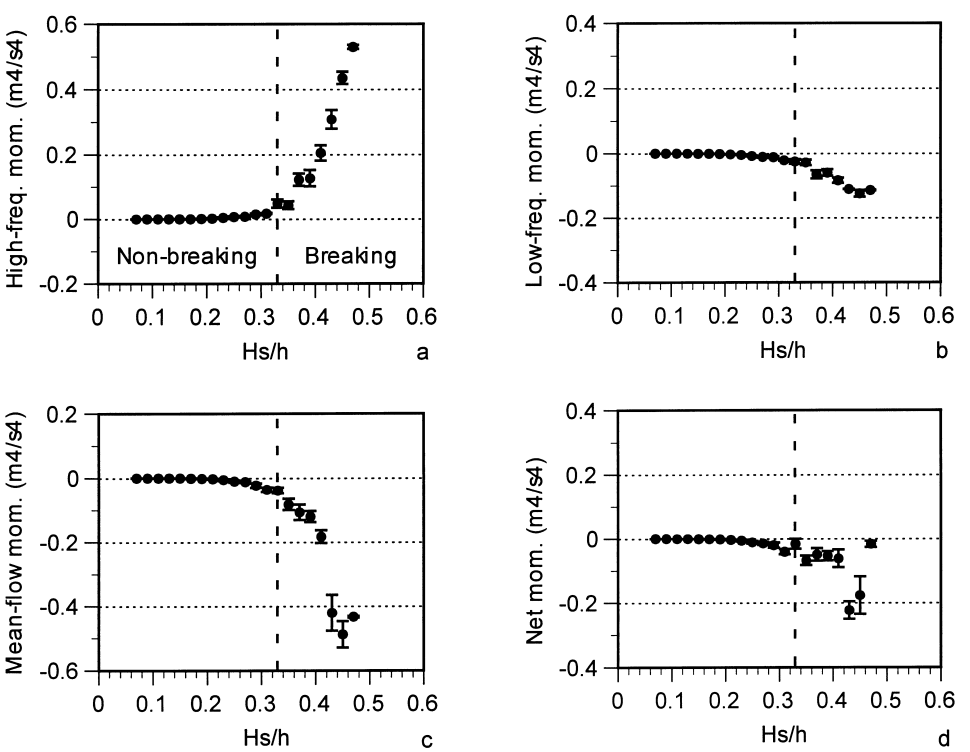

Fig. 10. The magnitude of (a) the high-frequency, (b) the low-frequency, (c) the mean-flow, and (d) the net fourth-order velocity moments at P1 as a function of the local relative wave height H_s/h. The vertical line through each class-mean value is the standard deviation. The vertical dashed line in each plot marks the onset of breaking ($H_s/h = 0.33$).

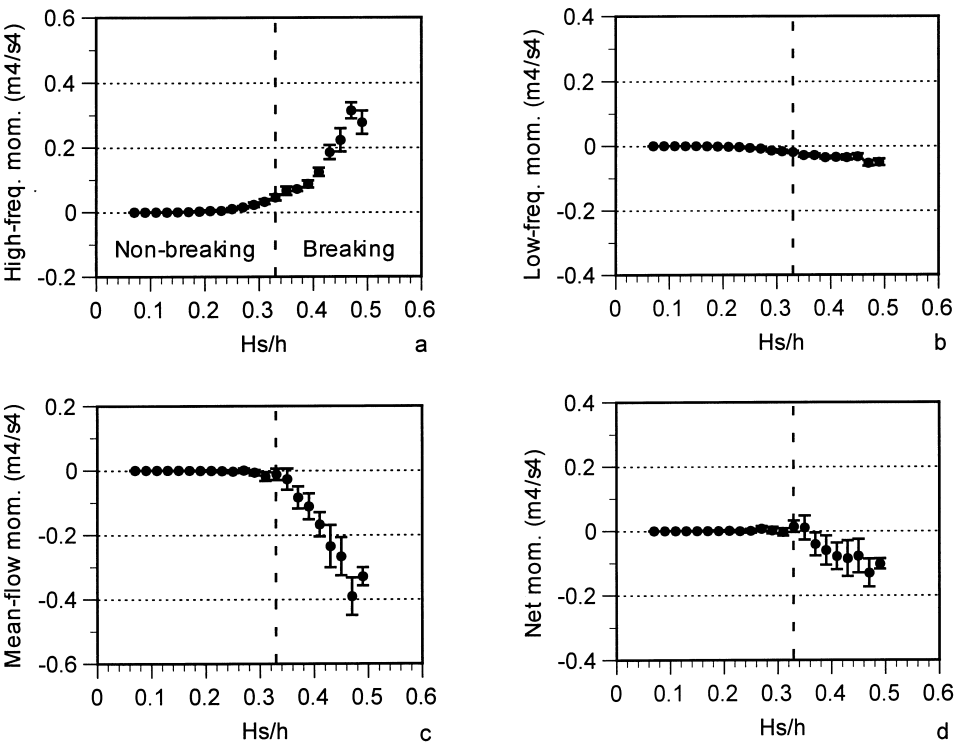

Fig. 11. The magnitude of (a) the high-frequency, (b) the low-frequency, (c) the mean-flow, and (d) the net fourth-order velocity moments at P2 as a function of the local relative wave height H_s/h. The vertical line through each class-mean value is the standard deviation. The vertical dashed line in each plot marks the onset of breaking ($H_s/h = 0.33$).

ues less than 0.33. Apparently, the cross-shore mean flow under non-breaking conditions was very small and did not result in a prevailing transport direction. In contrast, the mean moments had negative (offshore) values when P1 and P2 experienced surf zone conditions, related to the wave-driven undertow (see Section 4.1). A more scattered picture emerged at P3 (Fig. 12c), which is not unexpected because of the occurrence of both onshore and offshore flows under breaking wave conditions at P3 during the T2-campaign (see Section 4.2). The resulting trends of the mean-flow moments were comparable again to those at P1 and P2, when the categorising into H_s/h classes at P3 was restricted to the T3-data (e.g., compare Fig. 12e with Fig. 10c and Fig. 11c). By only considering the T3-data the onshore currents with unknown origin observed during the T2-campaign were omitted from the analysis. In the deep middle trough at P4 none of the suspended load moments was systematically related to H_s/h (Fig. 13), which corresponds to the observations of the suspended fluxes in Fig. 8. The findings at P4 are therefore not further discussed in the remainder of this paper.

In general, the mean-flow moment at P1, P2 and P3 was of comparable magnitude to the high-frequency term. Thus, despite the increase in breaking intensity, the growth in the mean-flow moment was counteracted by an about equal rise in the short-wave oscillatory moments. In other words, under breaking conditions the amount of sand transported offshore by the undertow was opposed by an approximately equal amount moved onshore by the wave asymmetry. Clearly, the predicted depth-averaged suspended transport is a delicate balance between two large components of approximately equal magnitude, but of opposite sign. From this viewpoint, even a systematic contribution of a small velocity moment, such as related to forced infragravity waves, may not be neglected. The fact that the average value of the net moment was generally close to that of the low-frequency term (e.g., compare Fig. 10b and d) substantiates this further.

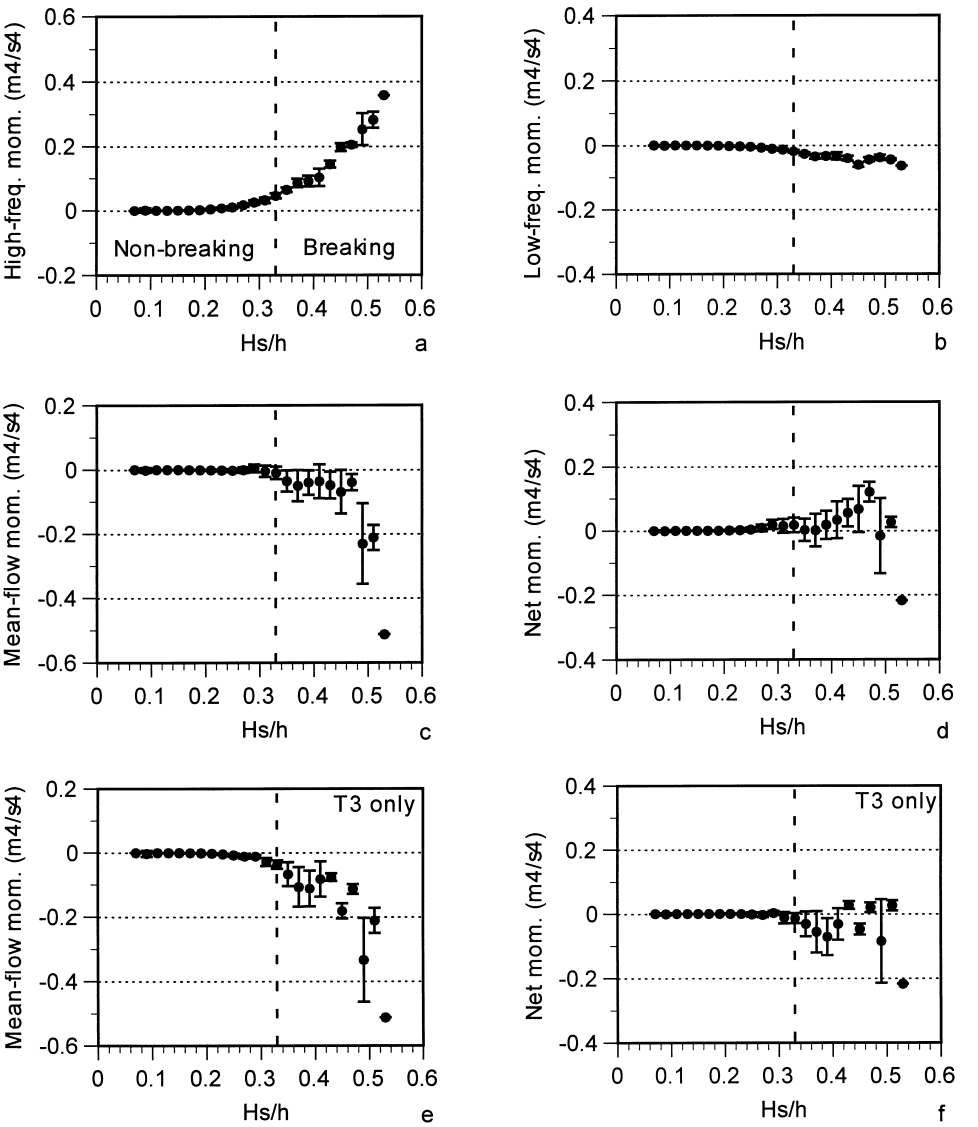

Fig. 12. The magnitude of (a) the high-frequency, (b) the low-frequency, (c) the mean-flow (T2 and T3-data), (d) the net (T2 and T3-data), (e) the mean-flow (T3-data only), and (f) the net (T3-data only) fourth-order velocity moments at P3 as a function of the local relative wave height H_s/h. The vertical line through each class-mean value is the standard deviation. The vertical dashed line in each plot marks the onset of breaking ($H_s/h = 0.33$).

Finally, it is noted here that Ruessink (1998a) performed a test to check the sensitivity of the present model findings to the reference level in the computation of the mean-flow, and consequently, net moments. In this test the mean flow at $z = 0.25$ m was replaced by the mean flow at $z = 0.10$, 0.15 and 0.50 m computed with Eq. 4. The main result of the test was that the choice of z in the range from 0.1 to 0.5 m did not influence the sign of the net velocity moments. Moreover, the magnitude of the net moments remained considerably smaller than those of the mean-flow and the high-frequency moments. In other words, the main observation that the predicted suspended sediment transport rate was finely balanced between two large, opposing components and a single, smaller constituent remained unaltered.

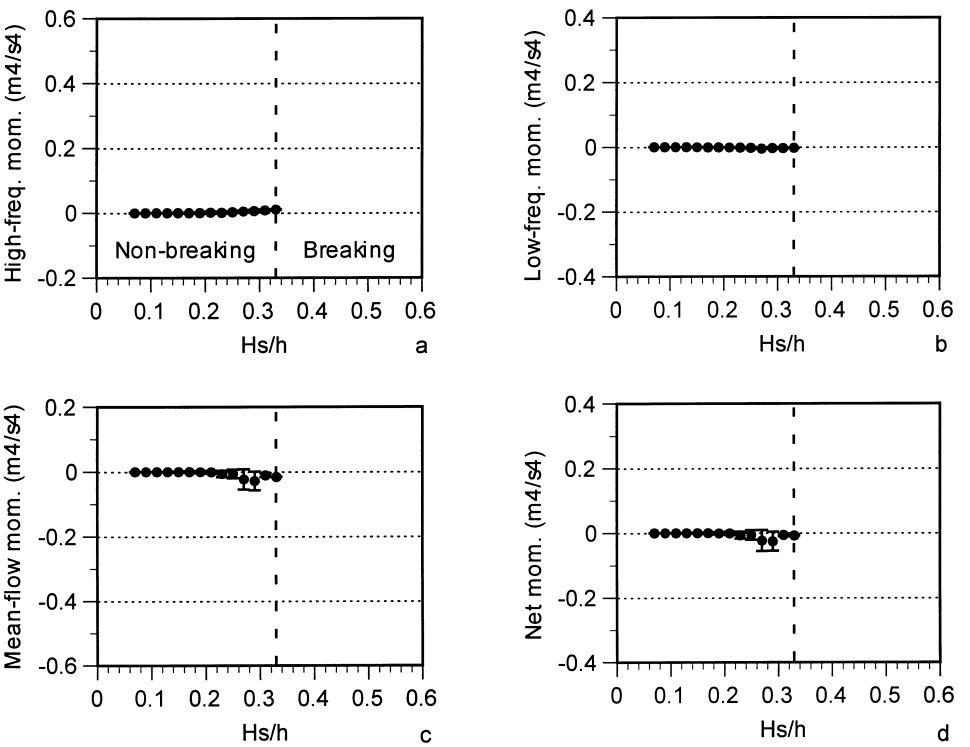

Fig. 13. The magnitude of (a) the high-frequency, (b) the low-frequency, (c) the mean-flow, and (d) the net fourth-order velocity moments at P4 as a function of the local relative wave height H_s/h. The vertical line through each class-mean value is the standard deviation. The vertical dashed line in each plot marks the onset of breaking ($H_s/h = 0.33$).

5.2. Contributions to the suspended load

The importance of a specific process to the cross-shore suspended sediment transport can be calculated as its relative contribution to the gross suspended sediment transport, analogously to Eq. 14. Values of the relative contribution of each transporting mode were, again, grouped according to $H_s/h \pm 0.01$. As such, the values are the relative contribution of a specific process to the gross suspended sediment transport within a H_s/h class. For example, a value of 0.2 for the infragravity contribution in the class $H_s/h = 0.33 \pm 0.01$ implies that 20% of the gross suspended sediment transport taking place during these conditions is due to infragravity waves. The contributions can be calculated in two different ways, namely by using (1) the individual and (2) the class-mean values as input. In the former approach the contributions were calculated for each measurement and at the end grouped into H_s/h classes. Thus it addresses the contributions of the various flows on the time scale of the individual measurements (say, hourly). In the latter approach, the velocity moments were classified first (i.e., Figs. 10–13) and the H_s/h grouped values were then used to calculate the contributions to the gross suspended sediment transport within the H_s/h classes. Because of the averaging of the velocity terms prior to the computation of the contributions the second method addresses the contributions on a larger time scale than that of the individual measurements. For instance, a sediment transport mode whose direction does not depend systematically on H_s/h will be averaged out over a sufficient long time period and its contribution in the second approach will therefore be minimal. Given the thousands of hours of available data, the time scale in the second method can be considered as the annual scale (see also Ruessink, 1998a). Figs. 14 and 15 show the relative hourly and annual contributions, respectively. As can be seen in the bottom row of Fig. 14, mean flows were the main factor in the gross suspended transport on an hourly scale during

low-energy, non-breaking conditions. The magnitude of the cross-shore currents amounted to only a few centimetres per second; they may have been the cross-shore component of the horizontal tide. It has to be kept in mind, though, that such values are probably within the measuring accuracy of the EMF. The two oscillatory components accounted for a larger part of the total load with increasing relative wave height, but still under non-breaking conditions. For example, the high-frequency transport even dominated the gross transport at P2 and P3 for the H_s/h range from 0.15 to 0.33.

The high-frequency oscillatory flow and the mean currents were of roughly equal hourly importance for situations with $H_s/h > 0.33$, with average contributions of about 0.4 to 0.5 (Fig. 14). The low-frequency oscillatory moment accounted for a much smaller portion of the gross suspended load (maximum of 0.2) and its importance reduced rapidly with increasing values of H_s/h. This is due to the destruction of the wave groups during breaking, which results in a less well-defined coupling between $|u_h|^3$ and u_l.

Although under non-breaking conditions the mean flow was the most important sediment transport process on the hourly scale (Fig. 14, bottom row), it barely contributed on the annual scale (Fig. 15 bottom row). This implies that the current-related transport under non-breaking conditions was not systematically related to the relative wave height, that is, it could both be onshore and offshore directed in the same H_s/h class. Note that the standard deviations of the yearly contributions (Fig. 15) for low-energy conditions were much larger than those of the hourly contributions. This is related to the fact that the standard deviations around the hourly class-mean values substantially exceeded the magnitude of the mean values themselves. This results in extremely large standard deviations around the mean medium-scale contributions.

The differences between the contributions of the three transport modes on the hourly and yearly scale were almost nil for $H_s/h > 0.33$. This denotes the systematic direction of the transports under breaking conditions. On the annual scale, the suspended sediment transport under breaking conditions was thus predicted to be mainly dominated by the short-wave asymmetry and the undertow. The annual contribution of bound infragravity waves to the gross suspended sediment transport in 3- to 9-m water depth was much smaller; it was largest under nearly breaking conditions (20–30%) and decreased rapidly with an increase in the relative wave height. The observed trends were comparable to those observed for the fluxes at the lower OBS (Figs. 5 and 7) with the two oscillatory components being slightly more important in the energetics approach.

5.3. A comparison between moments and fluxes

An easy qualitative check on the performance of the fourth-order velocity moments as predictors of the suspended sediment transport is to compare the measured fluxes to the corresponding moments. Note that the fluxes are point measurements at a specific height above the bed, whereas the moments reflect the depth-averaged suspended transport. Nonetheless, they should roughly exhibit the same trends. Fig. 16 shows the H_s/h classified fluxes observed at the height of the lower OBS-sensor at P2 plotted as a function of the corresponding classified moments. Only observations for $H_s/h \geq 0.29$ are shown, as the fluxes at lower relative wave heights were zero (Fig. 2). The best fit linear lines together with the regression parameters slope m and explained part of variance R^2 are shown in this figure as well. The regression line relating the mean fluxes and moments was strongly influenced by the single outlier point in the lower left part of Fig. 16c. Removal of this point resulted in the dashed regression line; the corresponding parameters are shown within brackets. All R^2 values are statistically significant at $\alpha = 0.05$.

The overall displayed resemblance between measured fluxes and moments is quite good ($R^2 > 0.7$). The scatter around the general trend lines is likely due to the sensitivity of the flux measurements for the sensor height above the bed. The slopes of the regression lines are comparable (taking the slope of the dashed line in Fig. 16c), which suggests that the relative weighting of the depth-averaged suspended sediment transport predicted by the velocity moments approach for $H_s/h \geq 0.29$ is similar to that based on the fluxes measured at the height of the lower OBS-sensor. In other words, the findings presented in Section 4 for $H_s/h \geq 0.29$ at the lower sensor were fairly representative of the depth-averaged con-

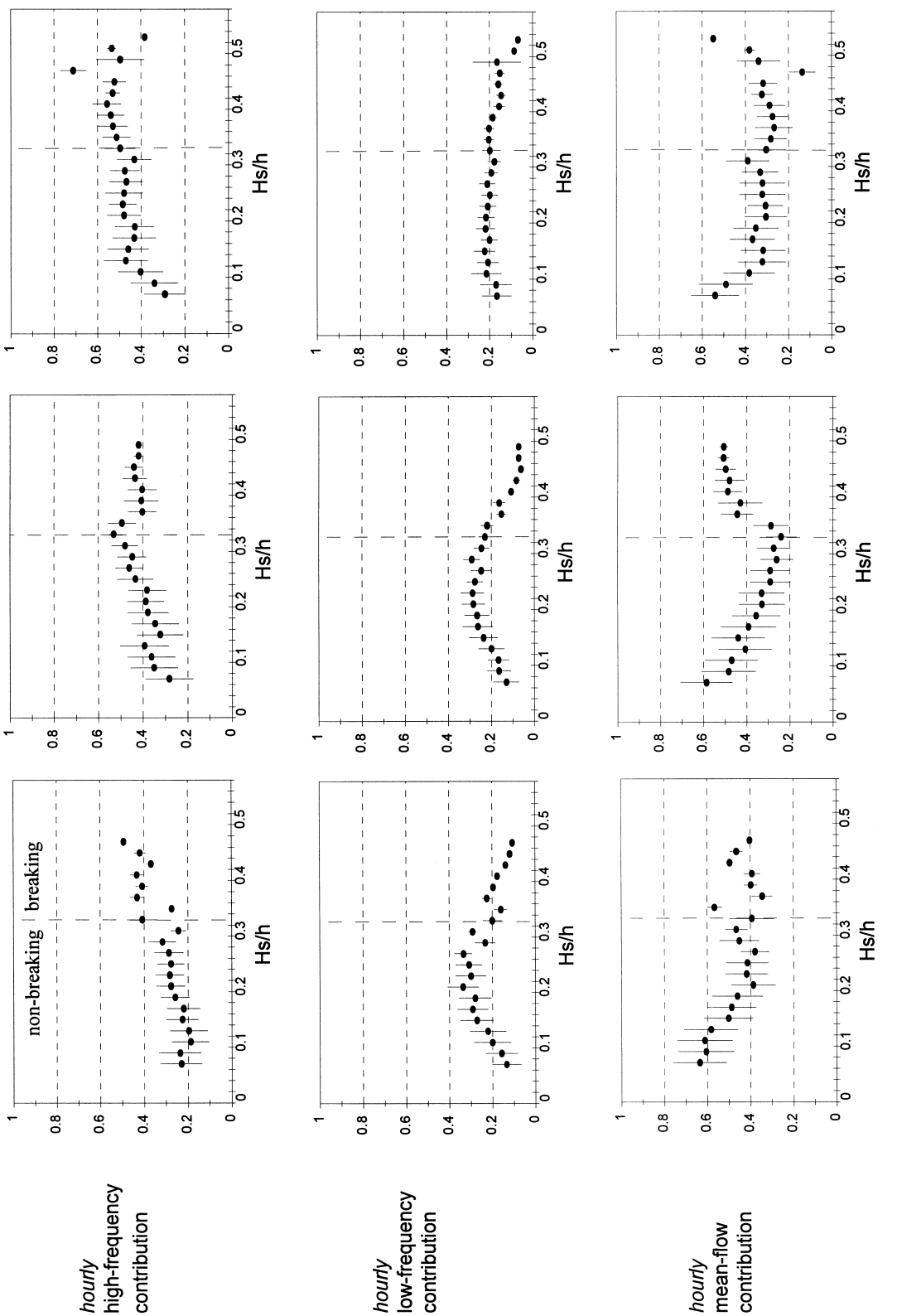
P1
P2
P3
non-breaking
breaking
hourly high-frequency contribution
hourly low-frequency contribution
hourly mean-flow contribution
Hs/h

tribution of the short waves, infragravity waves and mean flow to the suspended sediment transport. The intercept of the regression lines of the two oscillating flux components was non-zero (Fig. 16a and b). The velocity moments thus indicate that there was some depth-averaged suspended transport, whereas the measured high- and low-frequency fluxes at the lower sensor were still zero. It was shown in Section 4 (e.g., Fig. 2) that sand was only resuspended to the height of the lower sensor under conditions with a relative wave height of 0.29 or more. This threshold was even higher at the upper sensor, about 0.35. Inversely, this may imply that the suspended sediment transport was restricted to a layer close to the bed below the lower sensor during situations with relative wave heights less than 0.29. This may explain the non-zero intercepts in Fig. 16a and b.

Contrary to the positive values of the high-frequency moments, some of the measured local high-frequency fluxes at P3 were offshore directed (see Section 4.2). Reverse transports at short-wave frequencies, caused by phase shifts of 90 to 270 degrees between u and c, can obviously not be accounted for by the velocity moments approach, which assumes an instantaneous response of c to u. Several laboratory (e.g., Ribberink and Al-Salem, 1995) and field experiments (for instance, Kohanowich et al., 1995) have indicated that the majority of the high-frequency transport takes place close to the bed, where phase shifts between u and c are virtually negligible. At the same time, weaker, seaward-directed transports were revealed higher in the water column. From this viewpoint, the dissimilarity between local flux measurements at short-wave frequencies and moments at P3 should not be considered as a failure of the energetics expression (see also Russell et al., 1995).

6. Discussion

Energetics calculations presented in this paper suggest that at the present field site the suspended load dominates over the bedload (Fig. 9). The observed and estimated suspended load transport by short waves, infragravity waves and mean flows are all well related to the local height over depth ratio in 3- to 9-m water depth (Figs. 2, 6 and 10–12), apart from the deep middle trough (Figs. 8 and 13), where the estimated transports are independent of H_s/h. Under surf zone conditions the largest contributors to the suspended load are the onshore-directed, high-frequency oscillatory transport and the offshore-directed mean transport by the undertow. As both these transports are observed and predicted to be of approximately equal magnitude but of opposite sign, the net suspended transport may, rather paradoxically, be largely determined by the contributions of only a minor transporting mechanism, such as bound infragravity waves. From this viewpoint, a process that contributes to the gross suspended transport in only a subordinate way, should not be neglected. Summarising, if we want to model morphological coastal behaviour on the medium-scale (about years), then the small-scale transports to be considered are the suspended load transport by the skewness of the short waves, by the undertow and, probably, by bound infragravity waves. The bedload transport as well as the suspended load due to mean flows under non-breaking conditions seem to be of negligible importance.

It is now of interest to compare our findings to those of other field experiments, previously published in the literature. In all studies mentioned below, the contributions of short waves, infragravity waves and mean flows to the sediment transport were investigated with the energetics approach using measured time series as input. Wright et al. (1991) examined the cross-shore sediment transport in 7- to 9-m depth off the coast at Duck (USA); Wright et al.'s findings can best be compared with P1. The authors distinguished between fair weather, moderate energy, swell-dominated and storm conditions. The relative wave heights ranged from 0.06 to about 0.2, situations during which the transport potential at P1 was very small compared to those under breaking conditions (Fig. 10). Wright et al. found that small (<0.02 m/s) currents dominated the net transport

Fig. 14. The hourly contribution of short waves (top row), infragravity waves (middle row), and mean flows (bottom row) to the gross suspended sediment transport within H_s/h classes at P1, P2 and P3 (T2 and T3-campaign). The vertical line through each class-mean value is the standard deviation. The vertical dashed line in each plot marks the onset of breaking ($H_s/h = 0.33$).

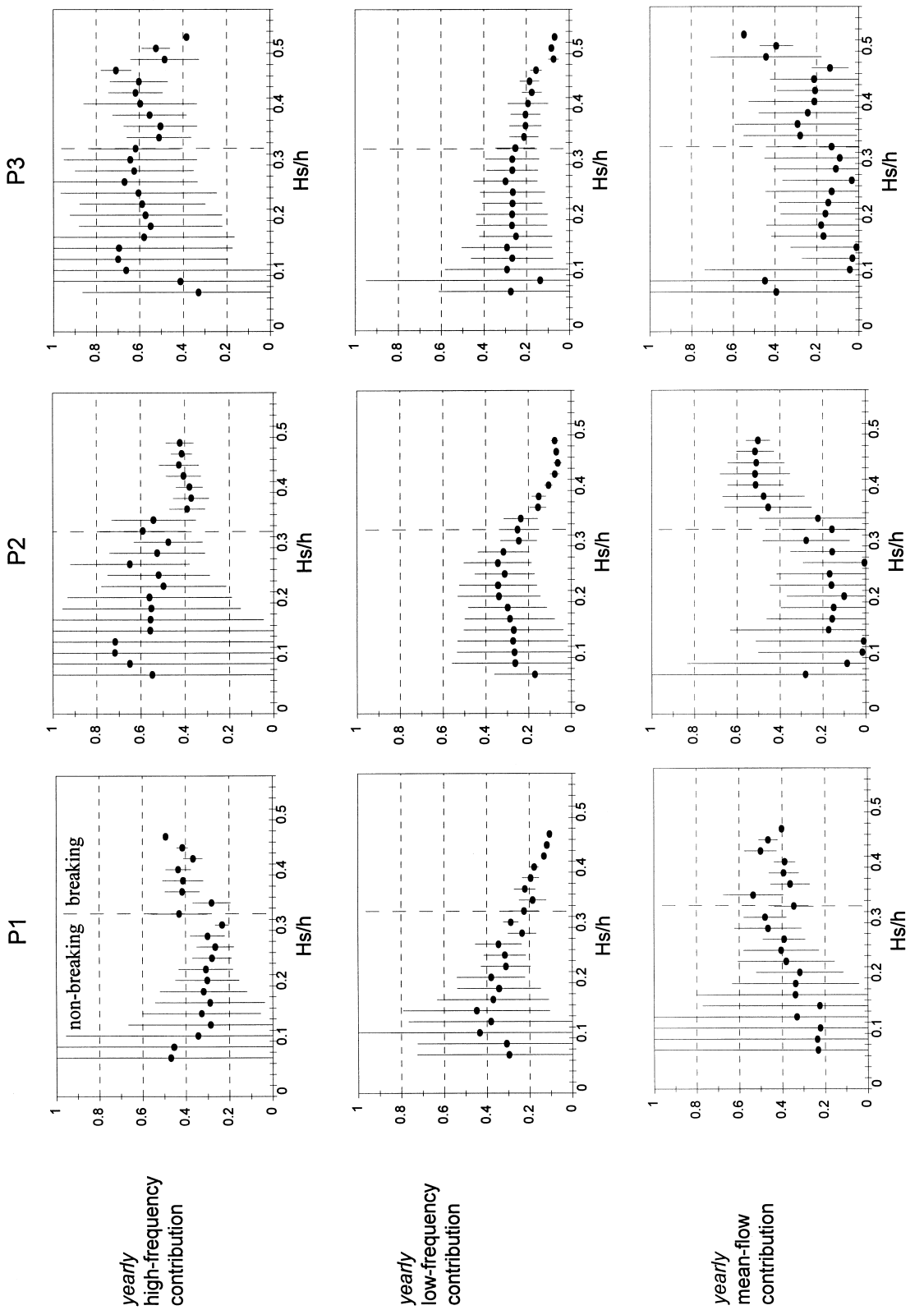
P1
P2
P3
non-breaking
breaking
Hs/h
yearly high-frequency contribution
yearly low-frequency contribution
yearly mean-flow contribution

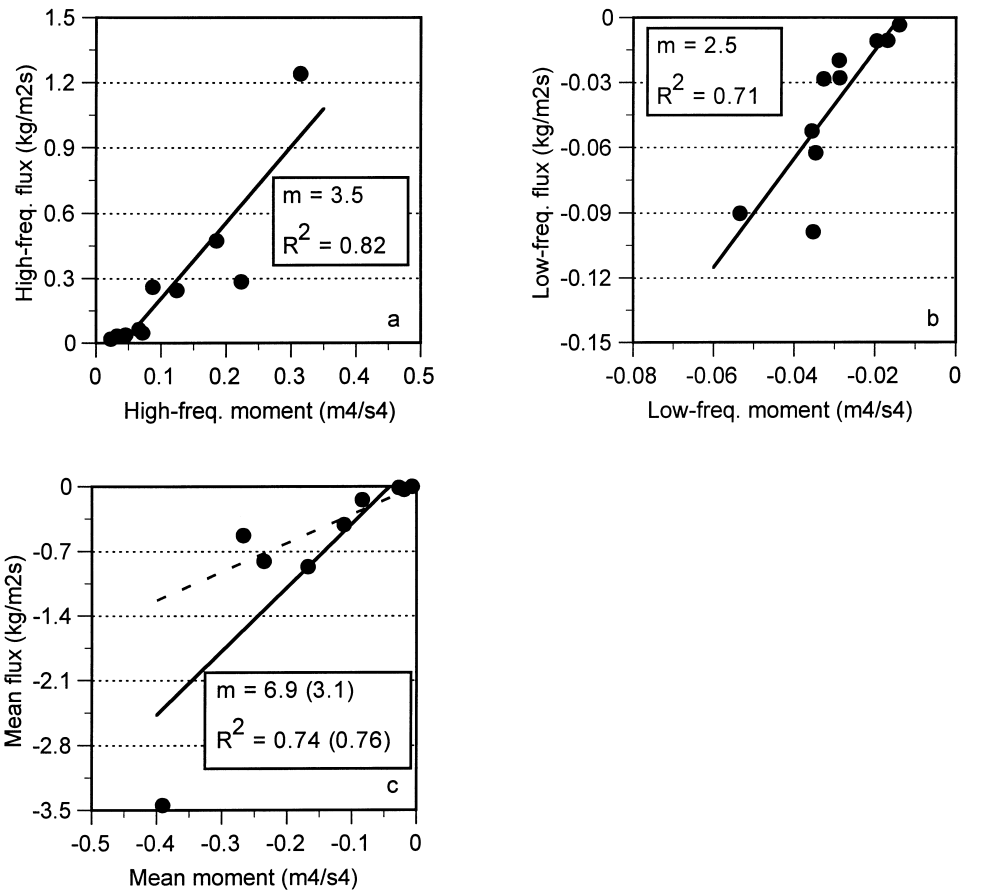

Fig. 16. Measured fluxes at P2 plotted as a function of velocity moments: (a) high-frequency, (b) low-frequency and (c) mean flow. The drawn lines are the best-fit linear lines. The dashed line in (c) is the regression line after removal of the outlier point.

on an hourly scale for $H_s/h \approx 0.06$, similar to P1 (Fig. 14). The bedload was predicted to be of comparable magnitude to the suspended load. The magnitude of the transports during storm conditions were, as expected, considerably larger and, as at P1, mainly due to the suspended load (see Fig. 9). The authors observed that infragravity-induced transport was only of a subordinate importance and could both be in a seaward and shoreward direction. An offshore directed current caused by wind-driven downwelling dominated the net flux. Such flows were not identified at the present field site.

Guza and Thornton (1985) conducted measurements at Torrey Pines Beach (California, USA) in depths ranging from 6 m to less than 1 m. The incident waves were mainly dominated by swell and had a significant height of about 0.7 m. As these authors did not divide the oscillatory velocity field into a high- and low-frequency part, the importance of infragravity-induced transport (both related to bound and free waves) cannot be assessed from their paper. They noted, however, that surf beat was too energetic to be ignored in sediment transport modelling, especially in depths less than about 2 m. Similar to the

Fig. 15. The yearly contribution of short waves (top row), infragravity waves (middle row), and mean flows (bottom row) to the gross suspended sediment transport within H_s/h classes at P1, P2 and P3 (T2 and T3-campaign). The vertical line through each class-mean value is the standard deviation. The vertical dashed line in each plot marks the onset of breaking ($H_s/h = 0.33$).

present findings, they observed the net transport to be a fine balance between onshore-directed oscillatory flow and the wave–mean current interaction term. They mentioned, however, that this finding should be interpreted with care given the possible large inaccuracies in the magnitude of the mean flow. Given the limitations in the measurements, Guza and Thornton considered suspended load and bedload to be of comparable magnitude for their range of encountered conditions.

Foote et al. (1992) presented measurements performed during three tidal cycles in less than 4-m depth in a macrotidal environment at Spurn Head (United Kingdom). The wave conditions ranged from a storm with local significant heights of 1.6 m to low-energy conditions with heights of only 0.8 m. Comparable experiments at various UK sites have been reported in Russell et al. (1995). In both these papers only bedload moments were presented. During non-breaking conditions the predicted infragravity-induced bedload transport was, as at the present site, related to the systematic concurrence of high values of $|u_h|^2$ and the troughs of bound long waves; it was of considerably smaller magnitude than the onshore-directed transport due to asymmetric short waves. In addition, they found mean flows under shoaling conditions to have a systematic onshore direction. Under breaking conditions infragravity waves were predicted to mobilise a significant amount of sediment, subsequently advected offshore by the undertow.

On the whole, our surf zone findings for $h \approx 3$ to 9 m differ markedly from those in much shallower water (say, $h < 2$ m) presented in the literature. In these depths, the undertow and infragravity waves seem to be main processes for the cross-shore sediment transport, with the importance of short waves diminishing rapidly with breaking intensity (for instance, Beach and Sternberg, 1991; Russell, 1993; Aagaard and Greenwood, 1994, 1995; Russell et al., 1995; Thornton et al., 1996; Gallagher et al., 1998). In 3- to 9-m depth bound infragravity waves seem to be the only contributors to the low-frequency transports, judging from observed and estimated offshore directed infragravity transports (Figs. 2, 6 and 10–12) and co-spectral shapes (e.g., Fig. 4b). Free long waves are randomly coupled to the group-enhanced stirring because of the broadbanded nature of the incident groups. Free infragravity motions may result in non-zero oscillatory transports when they suspend and transport the sediment themselves. This is obviously not the case here (e.g., Fig. 3). Another scenario for non-zero fluxes is the short-wave modulation due to the slowly varying depth caused by the long (standing) waves (Abdelrahman and Thornton, 1987; Aagaard and Greenwood, 1995). In case of depth limited breaking, higher (lower) short waves are expected on the crest (trough) of the infragravity waves, resulting in a positive coupling between the short-wave envelope and the long waves. At the four instrumented positions the coupling was either insignificantly different from 0 or negative due to presence of bound infragravity waves (Ruessink, 1998b). Moreover, full saturation of the short waves did not take place at the measurement sites. It appears that the second scenario is only of interest to shallower depths. For instance, Aagaard and Greenwood (1995) observed that in 2-m depth significant orbital velocities at incident frequencies could be up to 0.1–0.2 m/s larger for infragravity crests than for troughs. On the whole, it can be said that free infragravity waves do not contribute significantly to the oscillatory suspended sediment transport in 3- to 9-m depth.

In the present study the relative importance of processes for the sediment transport has been discussed in terms of magnitudes (i.e., point measurements), whereas the bars and their morphological changes are obviously the result of the gradients in the observed properties. Such gradients could not be studied with the present data because of the poor cross-shore resolution of the instruments (e.g., Fig. 1). The basic assumption that underlies the present work is that the magnitude of a transport process scales with the spatial gradient of that transport process. In other words, it is direct feedback between morphology, hydrodynamics and sediment transport that determines bar behaviour. Justification of this approach can be found by comparing the results at the middle bar crest (P3) and the middle trough (P4). Transport processes that induced large transports at the bar crest (i.e., sea-swell and undertow; see Fig. 12) resulted in almost negligible transports in the trough (Fig. 13), suggesting that gradients of both processes were large as well.

7. Conclusions

Near-bed hydrodynamics and sediment concentrations were measured at up to four cross-shore positions in 3- to 9-m depth in the multiple bar system of Terschelling for several thousands of hours. This large data set enabled us to look at the systematic contribution of short waves, infragravity waves and mean flows to the cross-shore suspended sediment transport.

Measured suspended sediment fluxes as well as predictions with an energetics-based sediment transport are well related to the relative wave height H_s/h, apart from the deep middle trough at P4. The model predicts that at the present site the bedload is of subordinate importance to the suspended load. Under surf zone conditions, the onshore-directed high-frequency oscillatory and the offshore-directed mean transport are observed and predicted to dominate the gross suspended transport. Infragravity waves, which induce a seaward directed transport because of the systematic coupling between bound-wave troughs and the enhanced stirring during the passage of a wave group, contribute only to a small degree; their relative contributions to the gross transports are, on average, less than 10–20%. The suspended sediment transport in 9-m depth, as well as at the seaward side of the outer and middle bar thus has to be considered as a delicate balance between two components of approximately equal magnitude but of opposite direction. Accordingly, the suspended transport of bound infragravity may not be neglected and may, rather paradoxically, largely influence the magnitude and direction of the suspended sediment transport. Summarizing, the transport to be considered in a process-oriented modelling of medium-scale morphodynamics in water depths of 3 to 9 m are the suspended load transport by the short waves, the undertow and, presumably, the bound infragravity waves. Transports that do not seem to be of importance are the bedload as well as the transports due to mean currents under non-breaking conditions and due to free infragravity waves. The agreement between the results of the flux measurements and the model predictions suggest that simple energetics models are suitable for predicting cross-shore sediment transport in the range of, at least, 3 to 9 m.

Acknowledgements

This work was carried out as part of the NOURTEC project: Innovative Nourishment Techniques Evaluation. It was jointly funded by the Ministry of Transport, Public Works and Water Management in the Netherlands and by the Commission of the European Communities, Directorate General for Science, Research and Development under the Marine Science and Technology programme contract No. MAS2-CT93-0049. We acknowledge the constructive comments received from Troels Aagaard and an anonymous reviewer, which improved the quality of the paper.

References

Aagaard, T., Greenwood, B., 1994. Suspended sediment transport and the role of infragravity waves in a barred surf zone. Mar. Geol. 118, 23–48.

Aagaard, T., Greenwood, B., 1995. Suspended sediment transport and morphological response on a dissipative beach. Continental Shelf Res. 15, 1061–1086.

Abdelrahman, S.M., Thornton, E.B., 1987. Changes in the short wave amplitude and wavenumber due to the presence of infragravity waves. Proc. Coastal Hydrodynamics, ASCE, New York, pp. 458–478.

Bailard, J.A., 1981. An energetics total load sediment transport model for a plane sloping beach. J. Geophys. Res. 86, 10938–10954.

Beach, R.A., Sternberg, R.W., 1991. Infragravity driven suspended sediment transport in the swash, inner and outer surf zone. Proc. Coastal Sediments '91, ASCE, New York, pp. 114–128.

Bowen, A.J., 1980. Simple models of nearshore sedimentation: beach profiles and longshore bars. In: McCann, S.B. (Ed.), The Coastline of Canada, Geological Survey of Canada, Ottawa, pp. 1–11.

Foote, Y.L.M., Huntley, D.A., Davidson, M.A., Russell, P.E., Hardisty, J., Cramp, A., 1992. Incident wave groups and long waves in the nearshore zone. Proc. 23rd Int. Conf. Coastal Engineering, ASCE, New York, pp. 974–989.

Gallagher, E.L., Elgar, S., Guza, R.T., 1998. Observations of sand bar evolution on a natural beach. J. Geophys. Res. 103, 3203–3215.

Guza, R.T., Thornton, E.B., 1985. Velocity moments in nearshore. J. Waterway, Port, Coastal, Ocean Eng. 111 (2), 235–256.

Hanes, D.M., 1990. The structure of events of intermittent suspension of sand due to shoaling waves. In: Le Mehaute, B., Hanes, D.M. (Eds.), The Sea, Vol. 9. Ocean Engineering Science, Wiley, New York, pp. 941–952.

Hanes, D.M., 1991. Suspension of sand due to wave groups. J. Geophys. Res. 96, 8911–8915.

Hanes, D.M., Huntley, D.A., 1986. Continuous measurements of suspended sand concentration in a wave dominated nearshore environment. Continental Shelf Res. 6, 585–596.

Huntley, D.A., Hanes, D.M., 1987. Direct measurement of suspended sediment transport. Proc. Coastal Dynamics '87, ASCE, New York, pp. 723–737.

Jaffe, B.E., Sternberg, R.W., Sallenger, A.H., 1984. The role of suspended sediment in shore-normal beach profile changes. Proc. 19th Int. Conf. Coastal Engineering, ASCE, New York, pp. 1983–1996.

Kohanowich, K.M., Stanton, T.P., Thornton, E.B., 1995. Acoustic sediment flux measurements from Duck '94. Proc. Coastal Dynamics '95, ASCE, New York, pp. 739–748.

Larsen, L.H., 1982. A new mechanism for seaward dispersion of midshelf sediments. Sedimentology 29, 279–283.

Longuet-Higgins, M.S., Stewart, R.W., 1962. Radiation stress and mass transport in gravity waves, with applications to 'surf-beats'. J. Fluid Mech. 13, 481–504.

Nairn, R.B., Southgate, H.N., 1993. Deterministic profile modelling of nearshore processes, Part 2. Sediment transport and beach profile development. Coastal Eng. 19, 57–96.

Ogston, A.S., Sternberg, R.W., 1995. On the importance of nearbed sediment flux measurements for estimating sediment transport in the surf zone. Continental Shelf Res. 15, 1515–1524.

Osborne, P.D., Greenwood, B., 1992. Frequency dependent cross-shore suspended sediment transport, 2. A barred shoreface. Mar. Geol. 106, 25–51.

Osborne, P.D., Greenwood, B., Bowen, A.J., 1990. Cross-shore suspended sediment transport on a non-barred beach: the role of wind waves, infragravity waves and mean flows. Proc. Can. Coastal Conf. 1990, NRC Canada, pp. 349–361.

Ribberink, J.S., Al-Salem, A.A., 1995. Sheet flow and suspension of sand in oscillatory boundary layers. Coastal Eng. 25, 205–225.

Roelvink, J.A., Stive, M.J.F., 1989. Bar-generating cross-shore flow mechanisms on a beach. J. Geophys. Res. 94, 4785–4800.

Roelvink, J.A., Meijer, Th.J.G.P., Houwman, K.T., Bakker, R., Spanhoff, R., 1995. Field validation and application of a coastal profile model. Proc. Coastal Dynamics '95, ASCE, New York, pp. 818–828.

Ruessink, B.G., 1998a. Infragravity Waves in a Dissipative Multiple Bar System. Ph.D. Thesis, Utrecht University.

Ruessink, B.G., 1998b. The temporal and spatial variability of infragravity energy in a barred nearshore zone. Continental Shelf Res. 18, 585–605.

Ruessink, B.G., 1998c. Bound and free infragravity waves in the nearshore zone under breaking and nonbreaking conditions. J. Geophys. Res. 103, 12795–12805.

Ruessink, B.G., Kroon, A., 1994. The behaviour of a multiple bar system in the nearshore zone of Terschelling, the Netherlands: 1965–1993. Mar. Geol. 121, 187–197.

Russell, P.E., 1993. Mechanisms for beach erosion during storms. Continental Shelf Res. 13, 1243–1265.

Russell, P.E., Foote, Y., Huntley, D.A., 1995. An energetics approach to sand transport on beaches. Proc. Coastal Dynamics '95, ASCE, New York, pp. 829–840.

Sallenger Jr., A.H., Holman, R.A., Birkemeier, W.A., 1985. Storm-induced response of a nearshore-bar system. Mar. Geol. 64, 237–257.

Shand, R.D., Bailay, D.G., 1998. A review of net offshore bar migration with photographic illustrations from Wanganui, New Zealand. J. Coastal Res. (in press).

Stive, M.J.F., 1986. A model for cross-shore sediment transport. Proc. 19th Int. Conf. Coastal Engineering, ASCE, New York, pp. 1550–1564.

Sunamura, T., Takeda, I., 1984. Landward migration of inner bars. Mar. Geol. 60, 63–78.

Thornton, E.B., Guza, R.T., 1982. Energy saturation and phase speeds measured on a natural beach. J. Geophys. Res. 87, 9499–9508.

Thornton, E.B., Humiston, R.T., Birkemeier, W., 1996. Bar/trough generation on a natural beach. J. Geophys. Res. 101, 12097–12110.

Van Enckevort, I.M.J., Reincke, E., 1996. Longshore currents in the intertidal zone of Terschelling. IMAU Report V96.09, Utrecht Univ.

Van Rijn, L.C., 1990. Principles of Fluid Flow and Surface Waves in Rivers, Estuaries, Seas and Oceans. Aqua Publications, Amsterdam.

Van Rijn, L.C., 1991. Database sand concentrations and sand transport in currents and/or waves. Report H1148-04/05, Delft Hydraulics, Netherlands.

Van Rijn, L.C., 1993. Principles of Sediment Transport in Rivers, Estuaries, Coastal Seas and Oceans. Aqua Publications, Amsterdam.

Wijnberg, K.M., Terwindt, J.H.J., 1995. Quantification of decadal morphological behaviour of the central Dutch coast. Mar. Geol. 126, 301–330.

Wright, L.D., Boon, J.D., Kim, S.C., List, J.H., 1991. Modes of cross-shore sediment transport on the shoreface of the Middle Atlantic Bight. Mar. Geol. 96, 19–51.